WL-TR-93-2128

FUNDAMENTAL STUDIES IN BLOW-DOWN AND CRYOGENIC COOLING

L. C. CHOW
W. F. LU
O. J. HAHN
M. S. SEHMBEY
M. R. PAIS

UNIVERSITY OF KENTUCKY
DEPARTMENT OF MECHANICAL ENGINEERING
LEXINGTON KY 40506-0046

SEPTEMBER 1993

INTERIM REPORT FOR 09/01/92-08/01/93

AEROPROPULSION AND POWER DIRECTORATE
WRIGHT LABORATORY
AIR FORCE MATERIEL COMMAND
WRIGHT PATTERSON AFB OH 45433-7650

NOTICE

When Government drawings, specifications, or other data are used for any purpose other than in connection with a definitely Government-related procurement, the United States Government incurs no responsibility or any obligation whatsoever. The fact that the government may have formulated or in any way supplied the said drawings, specifications, or other data, is not to be regarded by implication, or otherwise in any manner construed, as licensing the holder, or any other person or corporation; or as conveying any rights or permission to manufacture, use, or sell any patented invention that may in any way be related thereto.

This report is releasable to the National Technical Information Service (NTIS). At NTIS, it will be available to the general public, including foreign nations.

This technical report has been reviewed and is approved for publication.

Jeffrey R Brown

JEFFREY R. BROWN
Thermal Technology Section
Power Technology Branch
Aerospace Power Division

Jerry E Beam

JERRY E. BEAM, Section Chief
Thermal Technology Section
Power Technology Branch
Aerospace Power Division

Michael D Braydich

MICHAEL D. BRAYDICH, Lt Col, USAF
Deputy Chief
Aerospace Power Division
Aero Propulsion and Power Directorate

If your address has changed, if you wish to be removed from our mailing list, or if the addressee is no longer employed by your organization please notify WL/POOS, WPAFB, OH 45433-7251 to help us maintain a current mailing list.

Copies of this report should not be returned unless return is required by security considerations, contractual obligations, or notice on a specific document.

REPORT DOCUMENTATION PAGE

Form Approved
OMB No. 0704-0188

1. AGENCY USE ONLY (Leave blank)	2. REPORT DATE	3. REPORT TYPE AND DATES COVERED
	SEP 1993	INTERIM 09/01/92--08/01/93

4. TITLE AND SUBTITLE FUNDAMENTAL STUDIES IN BLOW-DOWN AND CRYOGENIC COOLING

5. FUNDING NUMBERS
C F33615-91-C-2152
PE 63218
PR 1601
TA 05
WU 03

6. AUTHOR(S)
L. C. CHOW
W. F. LU
O. J. HAHN
M. S. SEHMBEY
M. R. PAIS

7. PERFORMING ORGANIZATION NAME(S) AND ADDRESS(ES)
UNIVERSITY OF KENTUCKY
DEPARTMENT OF MECHANICAL ENGINEERING
LEXINGTON KY 40506-0046

8. PERFORMING ORGANIZATION REPORT NUMBER
UK-ME-93-04

9. SPONSORING/MONITORING AGENCY NAME(S) AND ADDRESS(ES)
AEROPROPULSION AND POWER DIRECTORATE
WRIGHT LABORATORY
AIR FORCE MATERIEL COMMAND
WRIGHT PATTERSON AFB OH 45433-7650

10. SPONSORING/MONITORING AGENCY REPORT NUMBER
WL-TR-93-2128

11. SUPPLEMENTARY NOTES

12a. DISTRIBUTION/AVAILABILITY STATEMENT
APPROVED FOR PUBLIC RELEASE; DISTRIBUTION IS UNLIMITED.

12b. DISTRIBUTION CODE

13. ABSTRACT *(Maximum 200 words)*

Experiments were conducted to study the free expansion (blow-down) behavior of cryogens. Visualization of the phenomena and determination of the final state of of LN2 during free expansion were the main purposes of the study. Results presented show the effect of nozzle size, upstream pressure and downstream pressure. The second part of the study details the experiments conducted to study the heat transfer characteristics during spray cooling with LN2. Four different nozzles at various pressures were used to study the variation in spray cooling heat transfer. Effect of nozzle and flow rate on the critical heat flux and overall heat transfer characteristics are presented. Finally an experiment designed to study the LN2 pool boiling heat transfer from discrete sources in a confined space is described.

14. SUBJECT TERMS
BLOW-DOWN, SUPERCRITICAL HYDROGEN, CRYOGENS, SPRAY COOLING, JET IMPINGEMENT, FREE EXPANSION, POOL BOILING

15. NUMBER OF PAGES
68

16. PRICE CODE

17. SECURITY CLASSIFICATION OF REPORT	18. SECURITY CLASSIFICATION OF THIS PAGE	19. SECURITY CLASSIFICATION OF ABSTRACT	20. LIMITATION OF ABSTRACT
UNCLASSIFIED	UNCLASSIFIED	UNCLASSIFIED	UL

TABLE OF CONTENTS

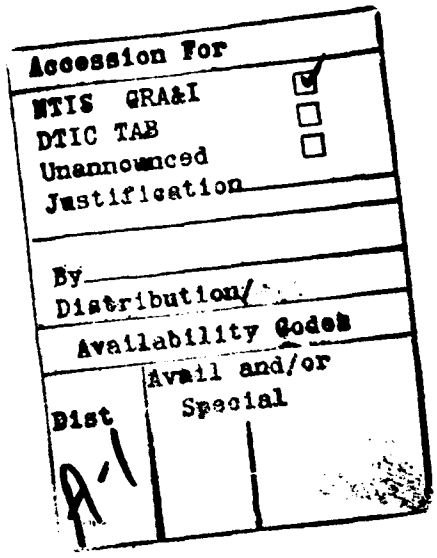

LIST OF ILLUSTRATIONS

NOMENCLATURE

d	Diameter of nozzle orifice
k	Thermal conductivity
l	Distance between thermocouples in copper block
l_2	Distance from top thermocouple to surface
$\dot{m}$	Mass flow rate
P	Pressure
Q	Heat
q''	Heat flux
T	Temperature
T_{sat}	Saturation temperature
T_{surf}, Tw	Heat transfer surface temperature
T_2	Temperature indicated by top thermocouple in the copper block
U	Internal Energy
W	Work
δ	Uncertainty
ρ	Density

1. INTRODUCTION

The operation of electronics at liquid nitrogen temperature (LNT) has become very attractive due to the development of high temperature superconductors and the fact that many MOS devices operate better at LNT. However, the information regarding the heat transfer characteristics of liquid nitrogen under various modes of heat transfer is not readily available. In order for the advantages of LNT operation of electronics to be realized, it is essential that enough information be available concerning the anticipated heat transfer modes.

This study involves the detailed investigation of heat removal methods for successful operation at LNT. In this respect, results from experiments conducted in spray cooling with liquid nitrogen (LN2) are presented here. Spray cooling was chosen as the first area of investigation because of its known capability as the highest heat flux removal method known. In order to examine the possibility of cryogenic cooling in space based systems, it is essential to study the free expansion (blow-down) process of cryogens. In this study, the liquid nitrogen free expansion was experimentally studied. The details of the study and the results are presented in the following chapters. This study will also involve the investigation of the pool boiling heat transfer to liquid nitrogen from multiple discrete sources in confined space.

The objectives of the study are detailed first, following that the background information for the motivation of this study is presented. The details of free expansion study containing the experiment details and results and discussion is presented next. The spray cooling study details are then presented, this contains details of the experimental results. The background and the details of the experiment set-up for the pool boiling study is presented after this. Finally, the conclusions and discussion for this report are presented.

2. OBJECTIVES

The objectives of this study are to obtain information on the heat transfer characteristics under the conditions of cryogenic cooling in various modes. Another objective is to evaluate the possibility of space based application for the various heat transfer modes. In order to accomplish the above, experimental data have to be obtained and analyzed for the heat transfer characteristics of LN2 under spray cooling, jet impingement cooling, forced convection cooling and pool boiling. In addition, experimental data are required for the phenomena involved in free expansion (blow-down) of cryogens into vacuum.

3. BACKGROUND

The electronic systems envisioned for LNT operations fall into two categories; first, the superconducting circuits composed of HTS devices, and second, hybrid circuits containing HTS and semiconductor devices.

3.1 Superconducting Circuits

Superconducting circuits will consist of HTS devices (logic gates, inverters, memory cells, etc.) with superconducting interconnects [1]. The main applications of the HTS circuits will be

a) High speed digital logic and memory: gate speeds under 10 ps are easily achievable using Josephson junctions [1-3]. This will allow the development of faster supercomputers.

b) Far infrared/high frequency radar detection: very low noise detection in the microwave and millimeter wave band is possible using Josephson junction device mixers; well above 100 GHz detection is possible with noise figures lower than 0.3 [1,4,5].

c) Magnetic field sensors: very sensitive magnetometers and voltmeters can be made using SQUIDs (Superconducting Quantum Interference Devices) [1,6,7]. This ultrasensitive instrumentation is used for magnetic field geophysical exploration and biomagnetic studies of human body.

Almost all of the functions performed in high performance electronics can be done by a superconductor circuit [2]. However, the superconductor circuits cannot handle high power levels, also, there are no superconducting rectifiers and semiconductors make better amplifiers and mass memory devices.

A cursory examination of heat transfer requirements in superconducting circuits may lead one to believe that due to the very nature of superconductivity heat dissipation would not be a problem. A closer examination, however, reveals how ill-founded that notion is. The main components in a superconducting circuit are the high speed, low power switches, the Josephson junctions (also called Superconductor-Insulator-Superconductor devices, SISs) [1-3, 8-10]. The main advantages of these devices are the low gate delay times and low power dissipation, these features in combination will allow much higher device packing compared to semiconductor circuits [1-3]. A typical SIS working at 4.2 K has a power dissipation of 5 W/cm^2, this depends

on the Josephson critical current density, J_c (2000 A/cm^2 at 4.2 K) and the gap voltage, V_g(4.5 mV for NbN which has T_c = 15 K) [9,10]. Hence, a circuit containing SIS devices operating at 4.2 K is easily handled by proper packaging and immersion in liquid helium. However, the gap voltage in SISs is directly proportional to the transition temperature of the superconductor [10]. Also, the critical current for the device will have to scale up in direct proportion to the operating temperature to ensure stable operation in presence of higher thermal noise [10]. This means that an SIS device operating at 77 K made from superconductor with T_c = 115 K will have V_g = 34 Mv and will have to operate at a critical current about 18 times higher than the device operating at 4.2 K. This can have two implications:

1) if the SIS device developed for 77 K operation has the same J_c as the low temperature one, then the size of the device will have to be scaled up to increase the total critical current, this will result in much larger device sizes and a power dissipation of about 68 W/cm^2, this option is not very attractive because larger device sizes will mean a loss in compactness and, hence, slower operating speeds
2) if the SIS device for 77 K operation are to be about the same size as the one designed for 4.2 K operation, the Jc will have to increase to about 18 x 2000 = 36000 A/cm^2, this results in a power dissipation of about 600 W/cm^2 (power = (V_g x J_c)/2, assuming equal times for on and off states of the switch)

Looking at the two options, we see that the first case can probably be handled by proper packaging and immersing the chip in LN_2 (pool boiling CHF $\simeq$ 15 W/cm^2), however, this option does not take advantage of SIS capabilities. The second option is the more attractive one if a way can be found to remove the power dissipated.

3.2 Hybrid Circuits

It has been reported by many investigators that MOS semiconductor devices show a marked improvement in performance as the operating temperature is lowered [1,2,8,11,12]. Furthermore, the thermal conductivities of semiconductor substrates and packaging materials (silicon, germanium, beryllium, alumina) are seen to increase dramatically as the temperature is lowered to LNT [13]. The main advantages of low temperature operation are: increased electron and hole mobilities, lowered interconnection resistivities, reduced leakage currents, greater subthreshold slope, more efficient heat dissipation, and reduction in thermal noise [11].

One of the possible applications of low temperature electronics will be in the area of high efficiency ac/dc, dc/ac and RF power conversion at the multikilowatt level. As mentioned earlier, superconducting circuits are not capable of handling high power levels. Hence, MOS field effect transistors (MOSFETs) can be used in combination with high Q inductors and capacitors made from HTSs to obtain the zero voltage switching circuits suitable for power conversion applications. Such an integration will result in a drastic size and weight reduction. The efficiency of these circuits improves greatly at low temperatures due to the dramatic reduction in the on-resistance of power MOSFETs [12]. However, the efficiency of these circuits depends greatly on the Q values of the inductors and capacitors used in the circuit. Hence, it is necessary to use HTSs for these components to obtain the maximum efficiency. The main hurdle is the development of these HTS components capable of handling high RF current densities [12].

Other types of hybrid circuits taking advantage of the best features of semiconductors and superconductors are also under development [1,2,8]. Any hybrid circuit is inherently more prone to thermal failure due to the presence of high heat dissipation transistors in the vicinity of superconducting elements. Hence, it is essential that the cooling system is capable of removing the heat very efficiently. This can probably be done by using bulky heat spreaders and immersing the circuit in LN_2, however, this reduces the size and weight advantage associated with a hybrid circuit. This again points towards the need to employ a high heat flux removal method.

3.3 Thermal Management of Circuits at LNT

The possible methods of high heat flux removal for LNT operation are; spray cooling, jet impingement cooling and forced convection boiling. The overall aim of this study is to undertake a comprehensive investigation of the heat transfer characteristics of these modes with LN_2 as the coolant. In spite of the advantages associated with high heat flux removal methods, their applicability is limited. The earliest applications of LNT operation will probably use pool boiling heat transfer to liquid nitrogen. Hence, in addition to the high heat flux methods, this study also involves the investigation of pool boiling heat transfer from a multiple heat source bank in a confined space.

In space based weapon systems, all the operating systems have to be brought from their idle state to full functionality within a few minutes. Thus, the heat transfer management system

has to be rapidly deployed. For cryogenically cooled power electronics, this will mean bringing up a system from vacuum state to cryocooled state in a very short time. Thus, the blow-down process for cryogens needs to be studied. In this regard, this study involves the examination of the free expansion (blow-down) process in cryogens.

4. FREE EXPANSION

An experimental set-up was designed and experiments performed to get a better insight into the thermal and fluid flow phenomena occurring in the blow-down tube (BT), and to obtain data which is critical to the performance of the system. The experimental objectives were:

1)observe the phenomena during the blow-down process

2)thermodynamically determine the final state

3)obtain knowledge about fluid instabilities in blow-down

4.1 Design Considerations

The thermophysical phenomena occurring in the flow field and within the walls of the blow-down tube are varied and complex. In order to be able to design and predict the operation

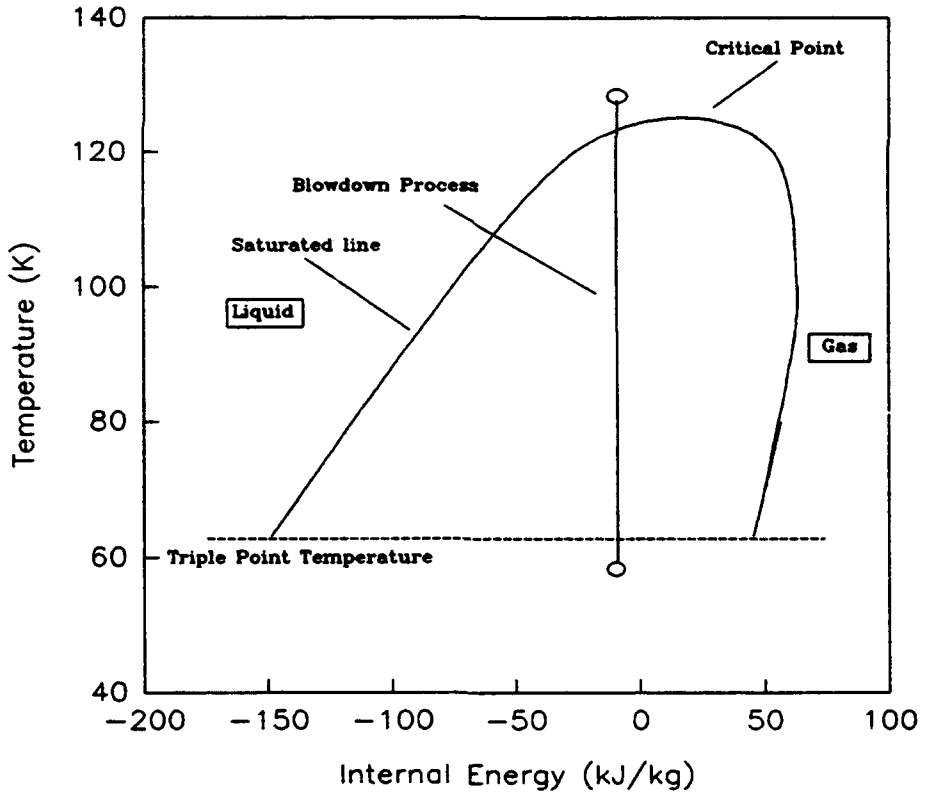

Figure 4.1 Blow-Down Process

characteristics of such a tube, careful considerations are needed. Without losing academic value, liquid nitrogen was used to substitute liquid hydrogen. To determine the physics of the blow-

down procedure, a scale-down model of a blow-down tube was used.

The main focus of the experiment was on the following categories:

1)Visualization: Figure 4.1 shows the thermodynamic path the blow-down process goes through. Since the final state region is below the triple point, it is expected that during the free expansion, nitrogen will freeze to form solid nitrogen. Also when nitrogen is near the triple point region, there will be two-phase flow, either solid-gas, or liquid-gas mixture will be seen in the blow-down tube. For nitrogen, the critical pressure is 500 psi. There exists a relatively big pressure drop during the blow-down process, hence, the liquid nitrogen will break and very small droplets. All these phenomena have never been described in previous research pa The experimental set-up, thus, had to allow direct visualization of the phenomena.

2)Measurements: The most important parameters to be measured were the pressure and the temperature of the initial and final state. The final state lies in the two phase region, hence the final state has to be thermodynamically determined. This is done based on the following analysis. The liquid nitrogen injector and the blow-down tube can be considered to be a closed system. The injector is under very high pressure (several hundred psi) while the blow-down tube is under vacuum. At the very far end of the tube exists a vent connecting to a vacuum pump that can be ignored for the short period of injection. The system can be treated as a close system at the instant of nitrogen injection. According to the first law of thermodynamics, the conservation of energy of the system can be written as:

$$Q=\Delta U+W \qquad \text{(Equation 4.1)}$$

Since the liquid nitrogen will undergo a free expansion process, there is no work done. Also at the instant of blow-down, the time span is so short that heat transfer can be ignored. Therefore, Q is equal to zero. The free expansion process can, thus, be regarded as a process where internal energy U remains constant. If the temperature and pressure of the upstream liquid nitrogen are measured, its internal energy can be determined. Then on temperature-internal energy diagram the final thermodynamic state can be determined, provided that its final temperature or pressure is measured.

Also, it is very important to measure the mass flow rate of liquid nitrogen in free expansion experiments. It provides critical data for determining the time needed for the cool-down process of the blow-down tube. This is the key problem in the start-up of the blow-down tube. Different

phenomena can also be compared between their corresponding flow rates.

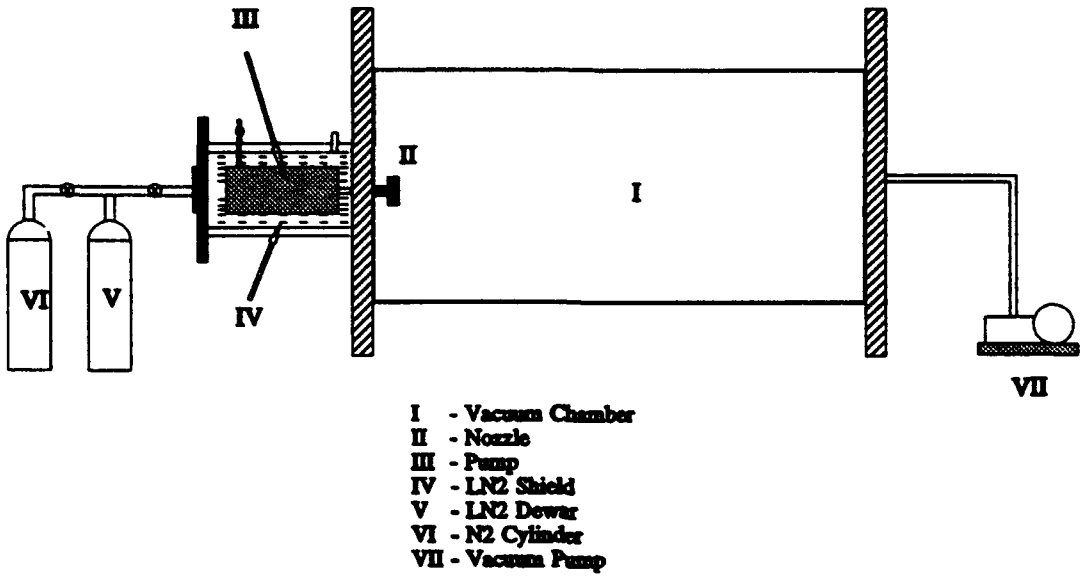

Figure 4.2 Schematic of Free Expansion Set-up

4.2 Design of the Experiment

Figure 4.2 is the schematic diagram of the experiment setup; it consists of five parts. Part I is the blow-down chamber. To make sure that the free expansion process can be seen and pictured clearly, a borosilicate glass cylinder was chosen to be the expansion chamber in this experiment. Borosilicate glass was selected because of its relatively high strength and small thermal expansion coefficient.

The critical pressure of nitrogen is 492.5 psia and the critical temperature 126.25 K. To ensure that the injector and the connecting pipes can handle the high pressure and extremely low temperature, stainless-steel 304 was chosen as the material to build the system. Stainless steel provides higher strength compared with other engineering materials. All the parts in cryogenic injector, connection tubes, nozzles, etc, were made of stainless-steel 304 in order to produce uniform contraction when they were under operation at cryogenic temperatures.

The pressure range of liquid nitrogen that the experiment would cover was from 100 psig to 500 psig. Since the experiment focuses on transient processes, the size of the experiment set-up should be as compact as possible to reduce thermal inertia. The blow-down process lasts about 30 to 40 seconds, assuming liquid nitrogen at 500 psig is injected into a perfect vacuum, and also assuming that there is no phase change during the process, the velocity of injection will be:

$$V_{N2} = \sqrt{\frac{2gp}{\rho_{N2}}} \qquad \text{(Equation 4.2)}$$

The liquid nitrogen can be treated as saturated. It gives the velocity of injection to be larger than 200 m/s. Suppose the injection period will last about 40 seconds, the volume of liquid nitrogen needed and the size of the blow-down nozzle can then be determined . Considering other requirements of the set-up, such as compactness, economy etc, the volume of liquid nitrogen per test cycle was chosen to be 50 cc and the size of nozzle range from 0.005 in to 0.014 in.

To achieve the very high pressure supercritical nitrogen (above 500 psig) requires, without losing compactness, a special arrangement was designed (Figure 4.3). The size of the pump was 1 in. in diameter and 6 in. in length (approximate volume 75 cc). To determine the diameter of the glass chamber (blow-down tube), the most important consideration is to allow the free

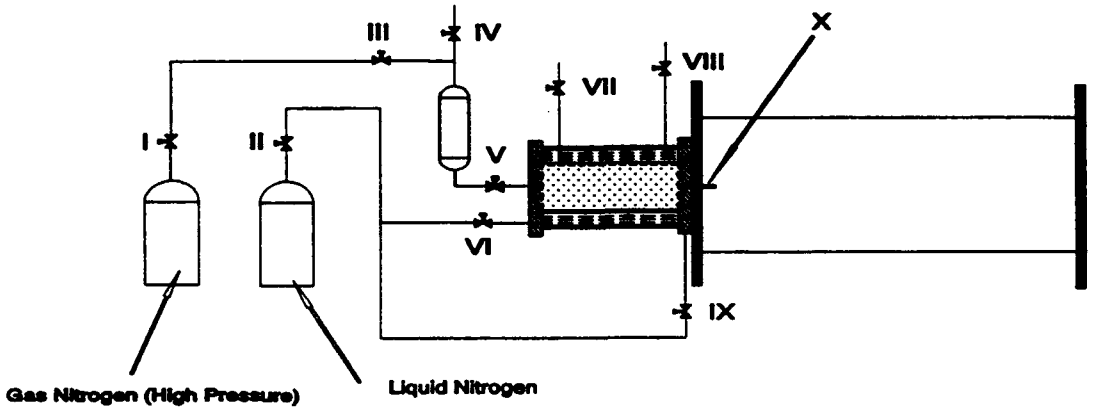

Figure 4.3 Pressurizing Arrangement

expansion phenomena to fully develop in the tube. The diameter of the glass tube was chosen to be 8 inches to allow an expansion rate of more than 600 times (diameter of the tube over that of the nozzle). The length of the glass chamber was chosen to be 40 inches based on the consideration that even when 75 cc of liquid nitrogen warms up to 300 K inside the chamber, the pressure inside the chamber should remain below atmospheric pressure.

The glass cylinder was sealed against the stainless steel flanges by two different methods. The warm side flange (i.e., the one connected to the vacuum pump) was sealed to the glass by a silicone O-ring, this was sufficient as the temperature on the warm side was not expected to go below the operating temperature of silicone. The seal between the cold flange and the glass was effected by an indium gasket, indium was chosen as the sealant because it remains soft and pliable below liquid nitrogen temperature. The seals between the various stainless-steel flanges were made using metal spring energized teflon O-rings; the details of the individual components and the assembly have been described in report No. UK-ME-92-06 [14].

Thermocouples were used to measure the temperature. The temperature of liquid nitrogen inside the pump was around 78 K, inside the glass chamber, the temperature ranged form 50 K to 300 K. For this range, E-type thermocouples were selected. The experiment dealt with transient process, so the response time of the thermocouples had to be as short as possible, in other words, their thermal inertia had to be small. Therefore, all the thermocouples used were self-made by welding the wires in an inert (Argon) environment. The diameter of the thermocouple wire was 0.003 in. and the thermocouple leads had teflon insulation.

Inside the glass chamber, six thermocouples were arranged in a row along the axis of the cylinder and nozzle. Thus, the thermocouples were in the trail of the liquid nitrogen spray ejected from the nozzle. There also was a pair of thermocouples inside the liquid nitrogen pump to measure the upstream temperature. Since the thermocouples were self-made, calibration was undertaken to ensure their accuracy. A special silicon-diode probe manufactured and pre-calibrated by LakeShore Inc. was used for the calibration. The silicon-diode probe has excellent repeatability: ± 10 mK at 4 K over repeated thermal cycling, and high accuracy: ± 0.5 K in 2K to 100 K range. The calibration set-up consisted of a nitrogen vessel and a vacuum pump. The vessel was filled with liquid nitrogen and subjected to different vacuum levels and the temperatures indicated by the thermocouples and the silicone-diode probe were compared for calibration. The calibration showed that the thermocouples were accurate to within 1 K in the

temperature range under consideration.

The pressure inside the glass chamber was measured by a convectron vacuum gauge connected to vacuum gauge controller (VGC). It can measure pressures from 1 x 10^{-3} Torrs to 1 atm. The pressure readout was available via the front panel display of the VGC along with an analog output proportional to the common log of the absolute pressure.

All measurement outputs were recorded by a computer via a Fluke Helios II data acquisition system. The thermocouples and pressure gauge output were hooked up to the data acquisition which was connected to the computer.

4.3 Experiment Procedure

Referring back to Figure 4.3, the liquid nitrogen storage tank was linked to the pump and the liquid nitrogen shield via a series of cryogenic valves. Valves II and VI are opened first to let liquid nitrogen flow through the cooling shield in order to precool the system. Vaporized nitrogen and air trapped in the cooling shell exits from valve VIII. In the meantime, the vacuum pump is switched on to evacuate the glass chamber. When the cooling shell is full of liquid nitrogen, valve IX and vent VII are opened to let the nitrogen fill the pump. Valve I, the pressure regulator of the nitrogen gas cylinder is adjusted to the desired upstream pressure. When the pressure inside the glass chamber drops to about 2 mmHg and the pump is full of liquid nitrogen, the vent valves are closed along with valve IX. Valve III is opened to pressurize the liquid nitrogen to the required pressure and valve X is opened to inject liquid nitrogen into the chamber. This process was repeated a few times to let the nozzle and the injector passage cool down. Then the pressure of the nitrogen gas is adjusted to 100, 200, 300, 400 or 500 psig (the pressures which were used for this study) and the procedure was repeated to obtain the pressure and temperature data.

The mass flow rate cannot be measured directly since it was two-phase flow. Hence, the average flow rate over 5 seconds of the injection was measured. The experiment procedure for flow rate measurement was similar to that described earlier for the blow-down experiments except the valve connecting the vacuum pump to the chamber was shut off before the injector valve was opened. The initial pressure and temperature inside the glass chamber was recorded. Then the injector valve is opened and sub/supercritical nitrogen is allowed to inject into the evacuated chamber for 5 seconds before the valve is shut off. The pressure of the chamber is

monitored and the final pressure is noted, usually the nitrogen gas inside the chamber reached room temperature. Assuming the gas nitrogen at this state as ideal gas, we can apply the state equation:

$$M_{N2}=\frac{PV}{RT} \qquad \text{(Equation 4.3)}$$

This gives us the total mass injected into the chamber in 5 seconds, the mass flow rate can, thus, be calculated.

4.4 Results and Discussion

Three different sizes of nozzles were tested, the upstream pressure of the liquid nitrogen were varied, from 100 psig to 500 psig for each nozzle. When the pressure inside the glass chamber was above the triple point, i.e., the pressure was higher than 98 mmhg, no freezing was observed. To simulate the conditions in space, the pressure of the blow-down tube was set to be as low as possible. Compared with the triple point of nitrogen which is 98 mmhg, the experimental chamber could go down to 1 or 2 mmhg, which was low enough for the purpose of this study.

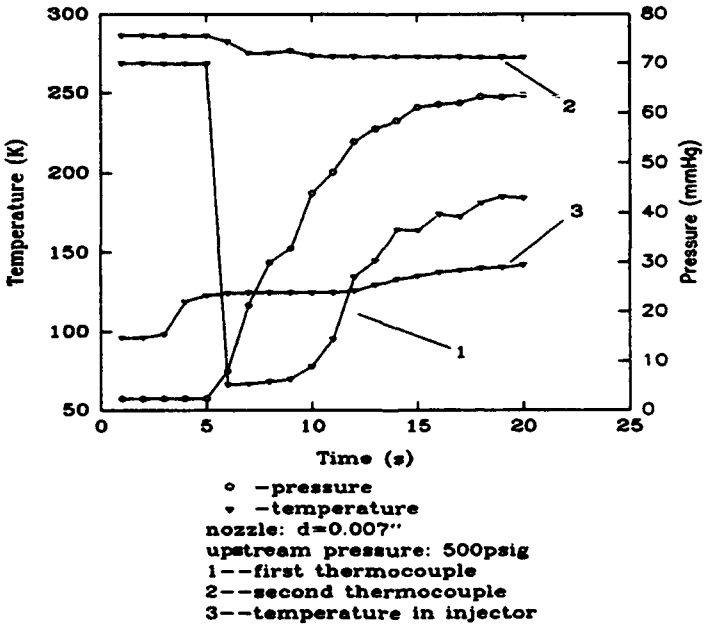

Figure 4.4 Temperature and Pressure in the Blow-Down Tube

The smallest size (0.007 in.) nozzle was tested first. When the injector valve was opened,

solid nitrogen appeared immediately at the nozzle orifice. It was very clear that the solid nitrogen was forming inside the nozzle since the solid nitrogen came out of nozzle very slowly, as if being pushed out of the nozzle by the pressure in the injector. The phenomena was much like squeezing a toothpaste tube. The solid nitrogen accumulated around the nozzle increasing in size as the experiment progressed. When the upstream pressure was low, i.e., 100 psig or 200 psig, the solid block could grow up to the size of 2 inches in length and 0.7 inch in diameter.

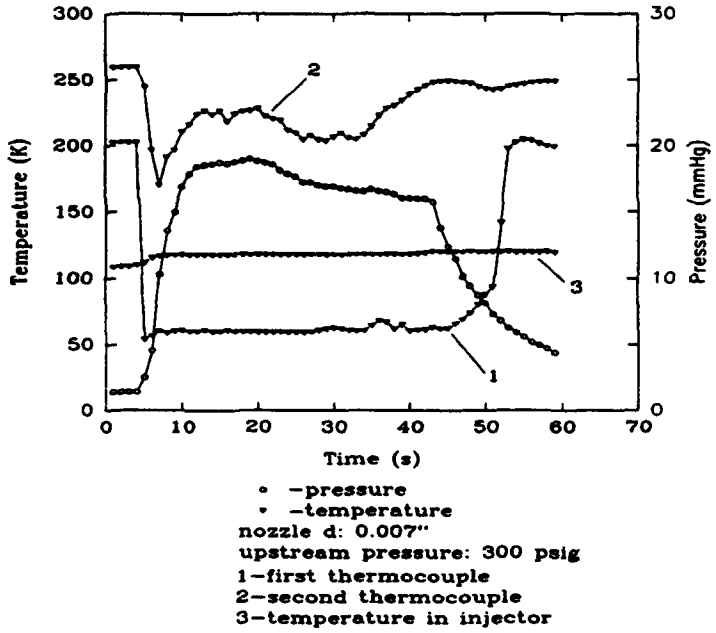

Figure 4.5 Temperature and Pressure in the Blow-Down Tube

The temperature of the solid was below triple point (64 K), the pressure inside the chamber rose to a certain level and remained stable because the solid block could not melt or sublimate quickly. When the ice block grew so big that it could not support itself anymore, it fell down to the bottom of the chamber. The temperature of the chamber wall was close to room temperature, hence, the block of solid nitrogen floated on the wall due to Leidenfrost condition. New ice block began to form on the rim of the nozzle after the previous block had dropped off.

When the upstream pressure was increased, the ice forming process seemed to accelerate; larger amount of solid nitrogen was pushed out of the nozzle. But since that the pushing force was larger, the solid block could not grow to the same size before it was pushed away. The size of the blocks became smaller while the frequency of generation of the solid blocks became

higher. This caused the pressure in the chamber to increase faster. The upstream pressure did not have strong impact upon solid formation process, it only effected the rate of solid ejection which is obviously proportional to the upstream pressure. The sublimation/melting process was very slow. The solid block could stay at the bottom of the chamber for a long time, usually until the experiment was ended. If the block did not fall to the bottom and touch the superheated wall, it would remain in solid form for a few minutes. Figures 4.4 and 4.5 show the temperature and pressure transients in the blow-down tube (the evacuated chamber) for upstream pressure of 500 psig and 300 psig, respectively. Figures 4.6 and 4.7 show the transient temperature field for the same two cases.

Experiments with the 0.010 in.-diameter nozzle were performed next. The solid formation phenomenon was very different in this situation. The solid nitrogen would form around the first thermocouple, there was a small distance between the nozzle exit and the thermocouple (about 1/8 in.). Spray could be seen very clearly, once the nitrogen droplets touched the thermocouple, solid accreted around the thermocouple. While the spray process went on, the ice block became bigger, but it could never reach the size of that formed around the small nozzle. Because the diameter of this nozzle was larger, the spray was much stronger too. When the pressure inside the injector was 300 psig, the ice block was blown away by the spray regularly. Since the block was small, it melted into liquid droplets once it touched the bottom of the chamber. The droplets floated on the wall due to Leidenfrost phenomenon. Figures 4.8 and 4.9 show the temperature and pressure transients in the blow-down tube for upstream pressures of 100 psig and 500 psig, respectively. The transient temperature fields for two cases are shown in Figures 4.10 and 4.11.

Finally, the 0.014 in.-diameter nozzle was tested in the system. In this case, the spray was much stronger. The solid nitrogen hardly formed before it was blown away; the ice block could grow to about 1 mm at the maximum. The thermodynamic parameters such as temperatures and pressures in the chamber were still similar to those of the other two nozzles. Figures 4.12 and 4.13 show the transient temperatures, pressure and the temperature field in the blow-down tube for an upstream pressure of 500 psig. The other results are included in the appendix along with photographs of the solid formation on the nozzle exit.

In order to determine the final point of the blow-down process in the glass chamber, temperature-internal energy diagrams were used. As the temperature and pressure in the injector were obtained, the initial internal energy could be determined. Since the blow-down process was

a constant internal energy process, as long as the temperature of the free expansion final state were measured, the final thermodynamic state could be located on the temperature vs. internal energy diagram. With increasing upstream pressure, the internal energy of the liquid nitrogen increases as well, therefore, the constant internal energy line shifts to the right as the pressure goes up. The experiments results on the temperature-internal energy diagram are shown on Figures 4.14, 4.15 an 4.16.

From Figures 4.6 to 4.13, it is clear that the cooling effect travelled along the glass chamber from the nozzle to the other end. Since the distances between each thermocouple could be measured accurately, the velocity of such cooling effect could be calculated. For the small nozzle the velocity is around 5 cm/s, when the upstream pressure increased, the velocity increased slightly. For the biggest nozzle, this velocity was up to 10 cm/s.

The mass flow rates of each different nozzle corresponding to various upstream pressures were obtained. The result is shown on Figure 4.17. According to fluid mechanics, flow rate of single phase fluid should be proportional to the square root of the pressure drop. The flow in the nozzle was two-phase flow which would not exactly obey the laws for single phase fluid. But the trend in flow rates was comparable.

From the experiments, it was obvious that the solid formation phenomena were very different when different types of nozzles were used. That is because the conditions for liquid nitrogen to form solid were quite different. The process of formation of solid nitrogen depends upon several parameters such as ambient temperature, droplet diameters, icing time and nozzle geometry. Among them, the most important factor that affects the phenomena of solid formation in this experiment is the nozzle geometry. When the length of the nozzle is relatively larger than its diameter, the nozzle is called *Tube Nozzle*. A nozzle is considered to be tube nozzle when its length is larger than seven times its diameter [15], i.e.:

$$\frac{Length}{Diameter} \geq 7 \qquad \text{(Equation 4.4)}$$

When tube nozzle was used in the system, the ice formed is called rime ice. Rime ice is a milky white, porous structure ice. It forms inside the nozzle. The pressure upstream of the nozzle was very high while the back pressure was only 2 to 3 mmhg. In this case, the liquid nitrogen flowing into the nozzle forms a flow pattern like the one shown in Figure 4.18. There exists a

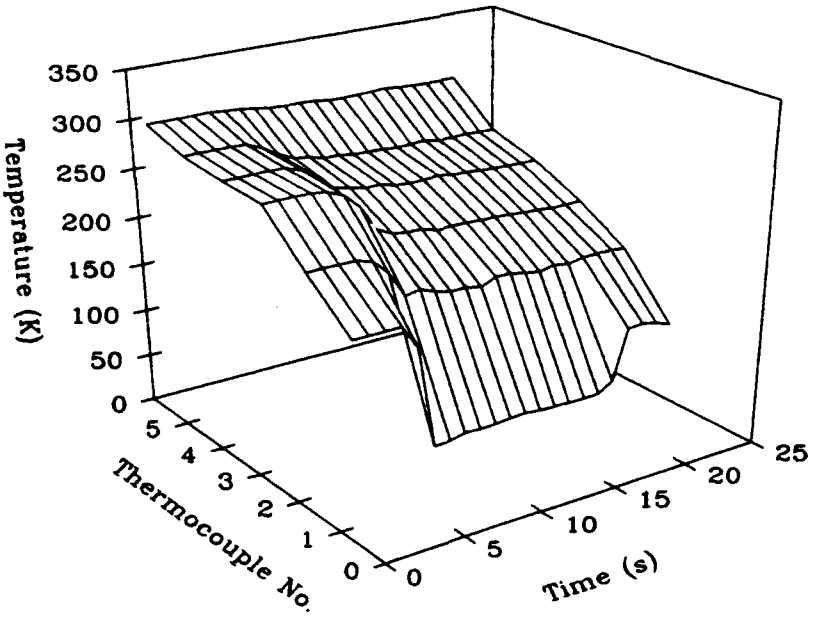

Nozzle: d=0.007"
Pressure in Injector: 300 psig

Figure 4.6 Transient Temperature Field

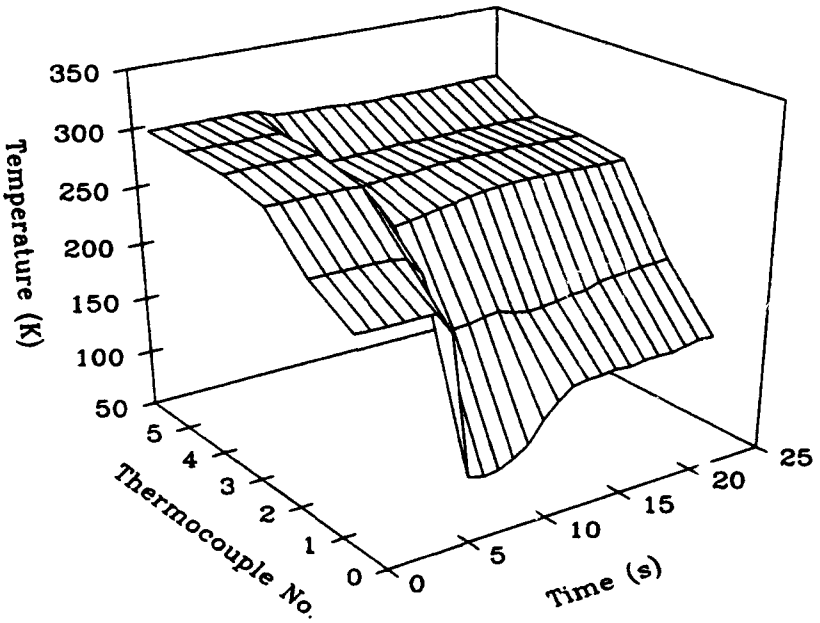

Nozzle: d=0.007"
Pressure in Injector: 500 psig

Figure 4.7 Transient Temperature Field

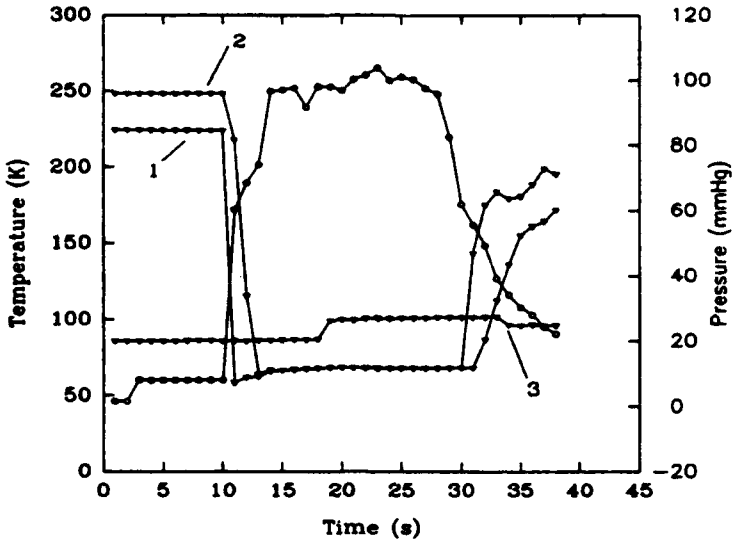

• –pressure
• –temperature
nozzle d: 0.010"
upstream pressure: 100 psig
1–first thermocouple
2–second thermocouple
3–temperature in injector

Figure 4.8 Temperature and Pressure in the Blow-Down Tube

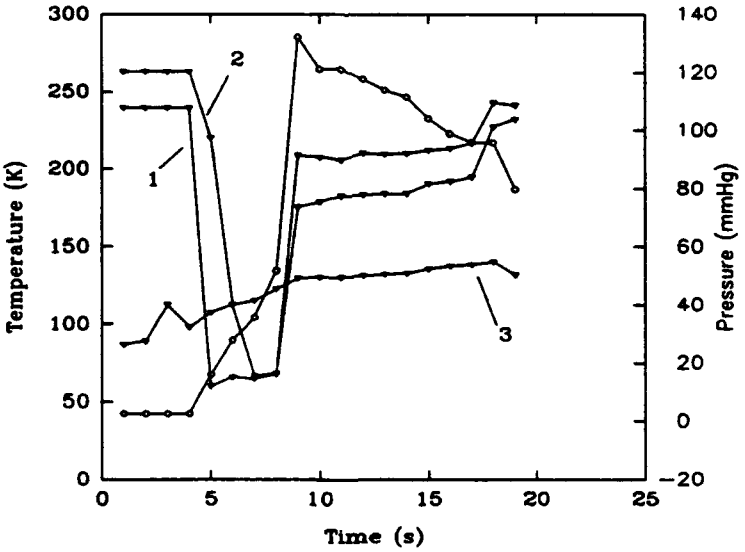

• –pressure
• –temperature
nozzle d: 0.010"
upstream pressure: 500 psig
1–first thermocouple
2–second thermocouple
3–temperature in injector

Figure 4.9 Temperature and Pressure in the Blow-Down Tube

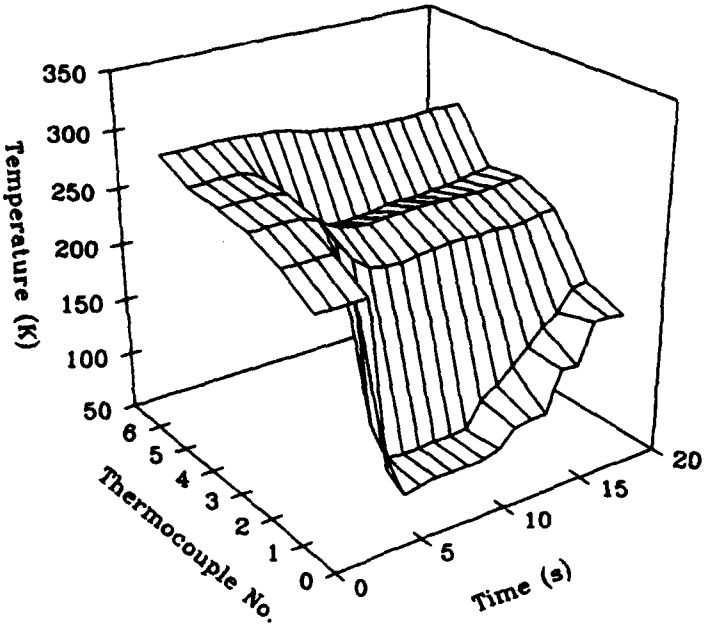

Nozzle: d=0.010"
Pressure in Injector: 200 psig

Figure 4.10 Transient Temperature Field

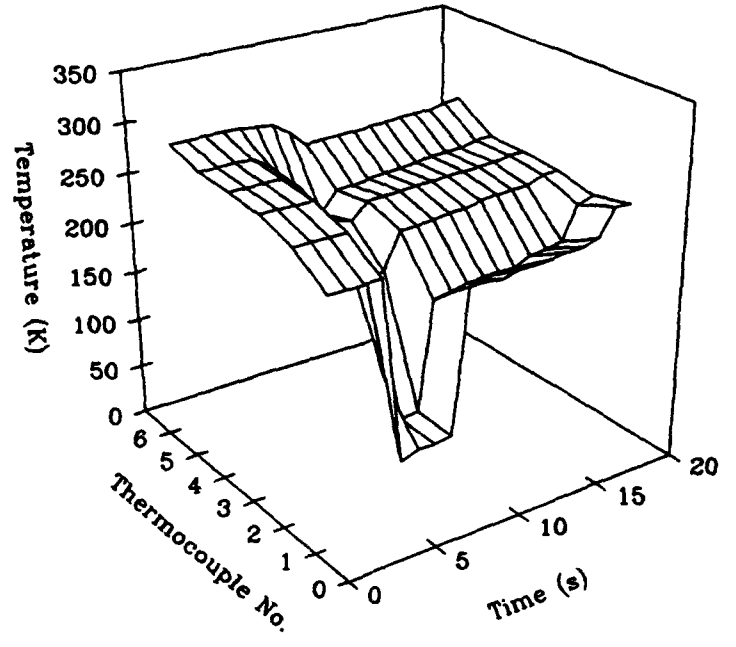

Nozzle: d=0.010"
Pressure in Injector: 500 psig

Figure 4.11 Transient Temperature Field

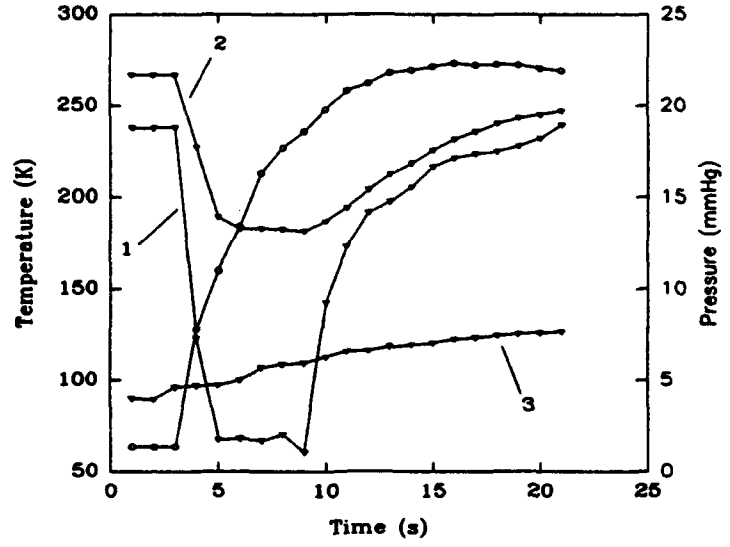

• –pressure
▪ –temperature
nozzle d: 0.014"
upstream pressure: 500 psig
1–first thermocouple
2–second thermocouple
3–temperature in injector

Figure 4.12 Temperature and Pressure in the Blow-Down Tube

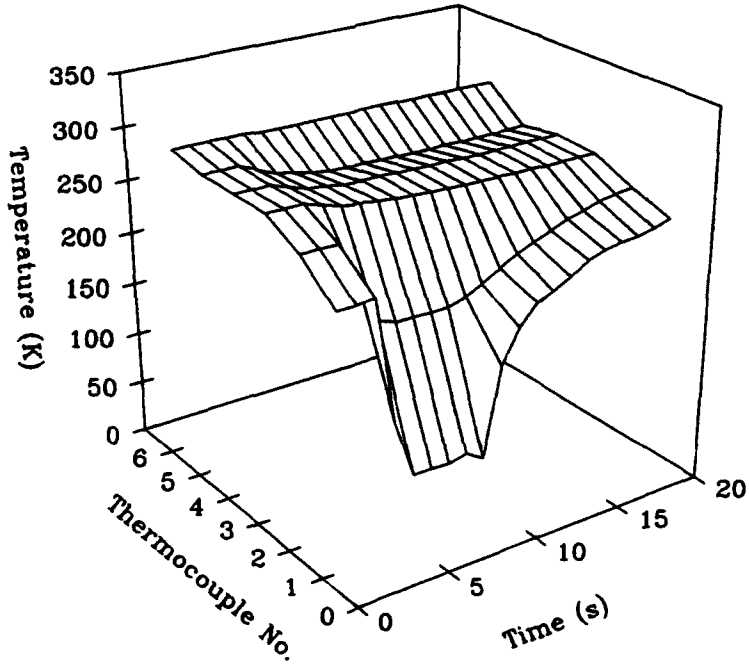

Nozzle: d=0.014"
Pressure in Injector: 500 psi

Figure 4.13 Transient Temperature Field

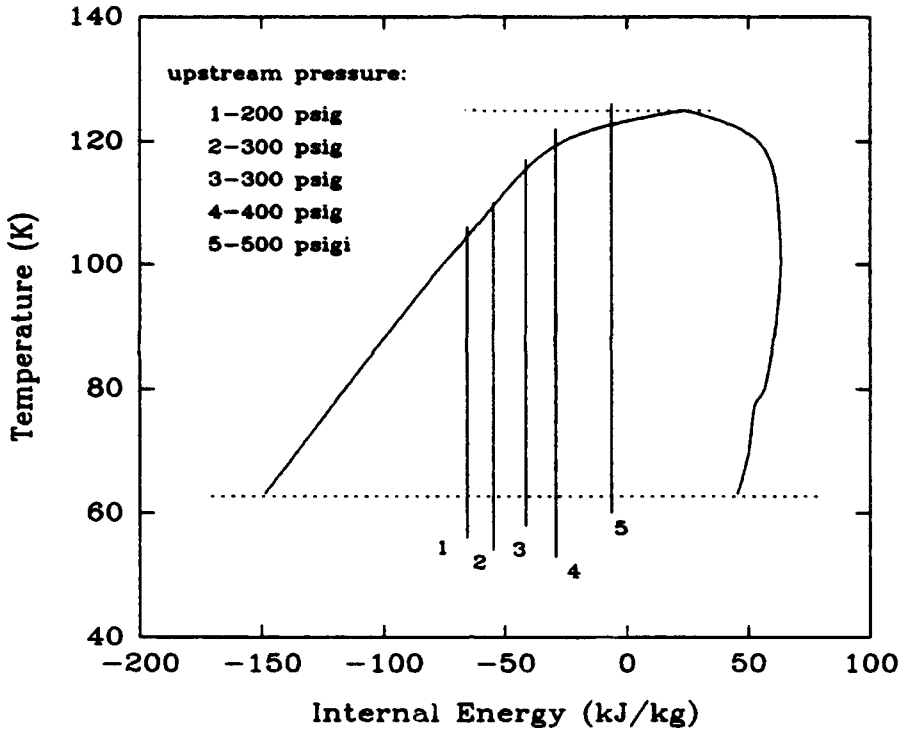

Figure 4.14 T-U Diagram for 0.007" Nozzle

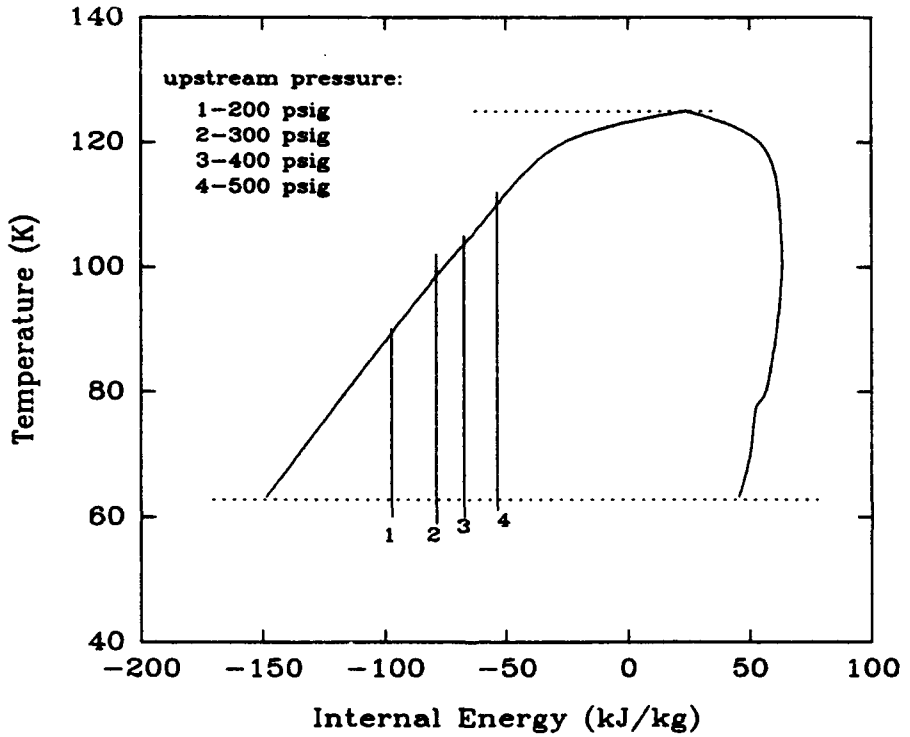

Figure 4.15 T-U Diagram for 0.010" Nozzle

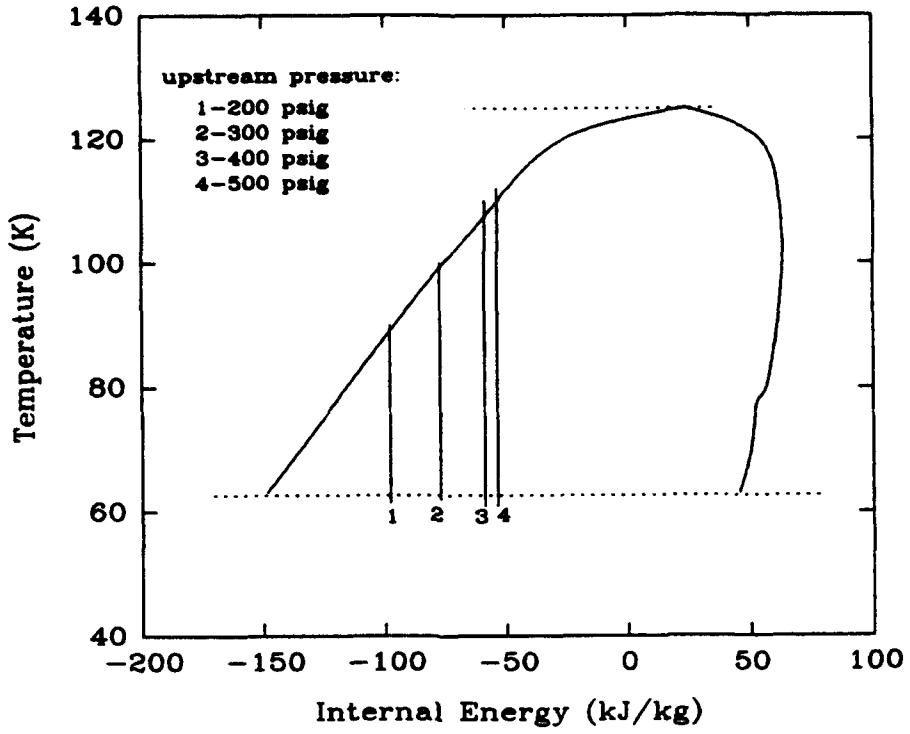

Figure 4.16 T-U Diagram for 0.014" Nozzle

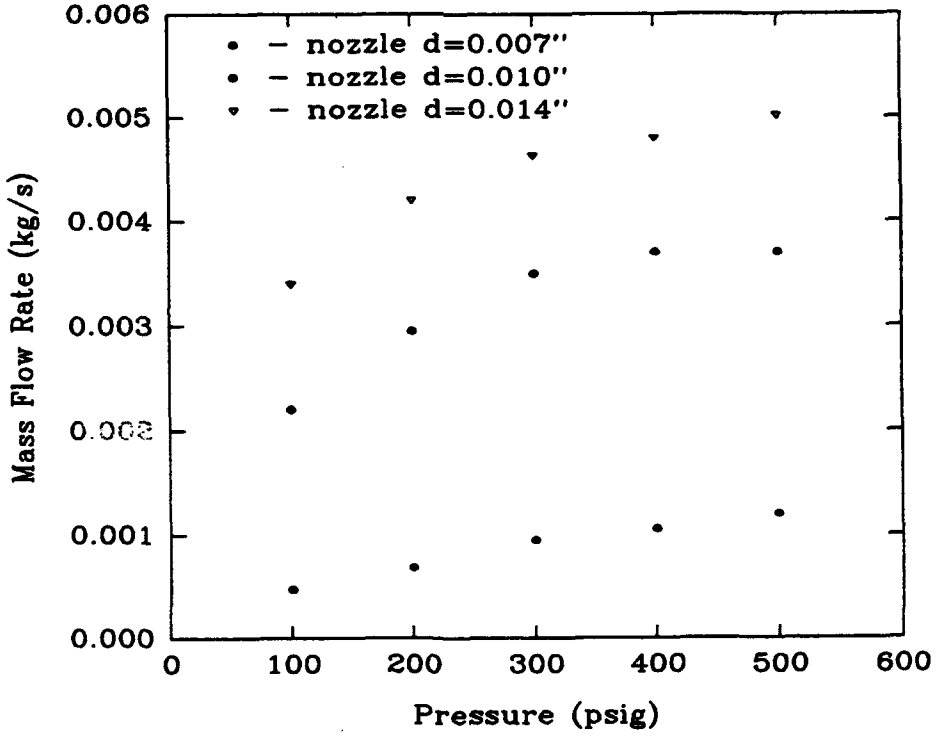

Figure 4.17 Mass Flow Rate

throttle condition inside the nozzle. The velocity of the nitrogen flow increases as the flow cross-section area becomes smaller. As a result, the pressure of the flow decreases, since the throttle was inside the nozzle, the triple point pressure would occur somewhere before the throttle plane which was inside the nozzle. Therefore, ice would form inside the nozzle and be pushed out of the nozzle by the upstream pressure. For the smallest nozzle in this experiment set-up, the diameter was 0.007 in. while its length was 0.055 in. The length of the nozzle is more than seven times as large as its diameter. Thus, the nozzle could be considered a tube nozzle. That is the reason for the observations during the experiment; it was clearly seen that solid nitrogen formed inside the nozzle and was pushed out.

The nozzles with diameters of 0.010 and 0.014 in. could not be considered as tube nozzle. They were ordinary straight nozzles, for these nozzles, there is no throttling inside the nozzle (Figure 4.18). In these cases, when liquid was sprayed into the glass chamber, it went through a process of sudden exposure to the vacuum. The liquid nitrogen droplets would form tiny solid droplets immediately. But neither the liquid nor the solid droplets could be seen since they were too small in size, so the phenomena appeared as a mist spray. The spray is, in fact, ice droplets spray. Liquid droplets turned into ice so fast that it could not be seen. The ice droplets hit the thermocouple and congregated around the thermocouple wire. During the experiments, it was being watched that ice growing around the thermocouple while the spray still going on. This process had been theocratically formulated and numerically solved.

The problem of freezing of liquid nitrogen upon a sudden exposure to vacuum has been studied in Reference [16]. Although the icing time, at which the process takes place, may vary slightly depending upon the pumping capacity and ultimate pressure attainable for the particular vacuum system, the icing time was very small for the situation in this study. The space environment can be regarded as a vacuum system with infinite pumping capacity and approximately zero ultimate pressure. An experiment was set up to simulate this condition, however, they found that the liquid nitrogen froze before it reached the nozzle exit.

The same study [16] showed that there existed a maximum stable drop diameter for liquid nitrogen, 2.7 μm when nitrogen at 77.4 K was subjected to sudden expansion. A temperature gradient within the droplet is established by cooling of the surface. The solid/liquid interface moves toward the center of the drop until the sphere became completely solid. The mathematic model dealing with the above situation is described in [16]. It shows that for liquid nitrogen

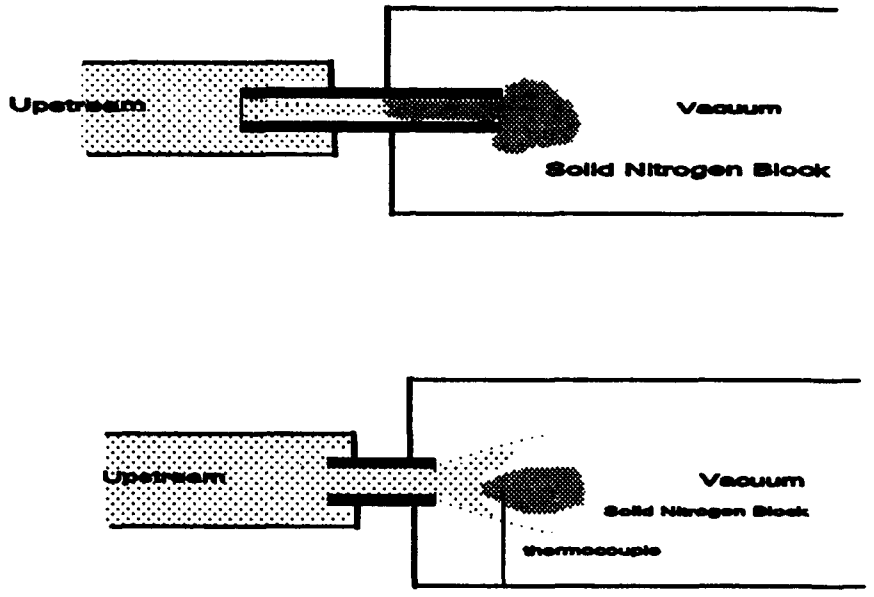

Figure 4.18 Solid Formation Process for Different Nozzle Sizes

freezing at triple point, the time required is less than 10^{-5} second. According to this, we can conclude that for the ordinary straight nozzle, tiny ice droplets were sprayed onto the thermocouple and accreted there.

5. SPRAY COOLING

The main objective of this part of the study is to obtain the heat transfer characteristics of liquid nitrogen spray cooling. This was done by obtaining heat transfer data for LN2 spray cooling under different spray conditions. The following sections describe the experimental set-up, procedure and results.

5.1 Experiment Set-up

The detailed design of the various parts of the experimental arrangement has been presented in report No. UK-ME-92-06 [14]. Hence, a brief description of the overall setup would be sufficient here. The schematic diagram of the set-up is shown in Figure 5.1. The experimental chamber contains the heater, nozzle and view ports for laser-Doppler velocimetry. The high pressure LN2 dewar is used to supply liquid nitrogen to the nozzle. A heat exchanger between

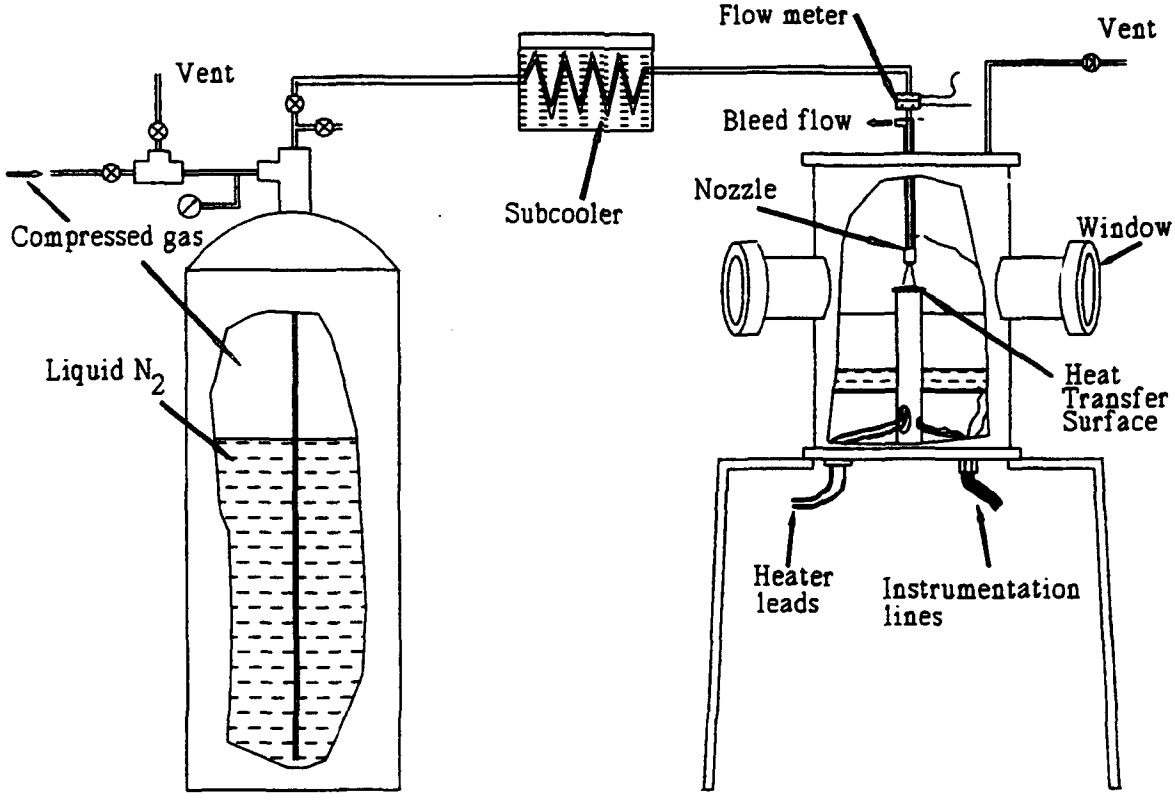

Figure 5.1 Experimental Set-up

the dewar and the nozzle is used to subcool the high pressure liquid down to about 78 K. Since

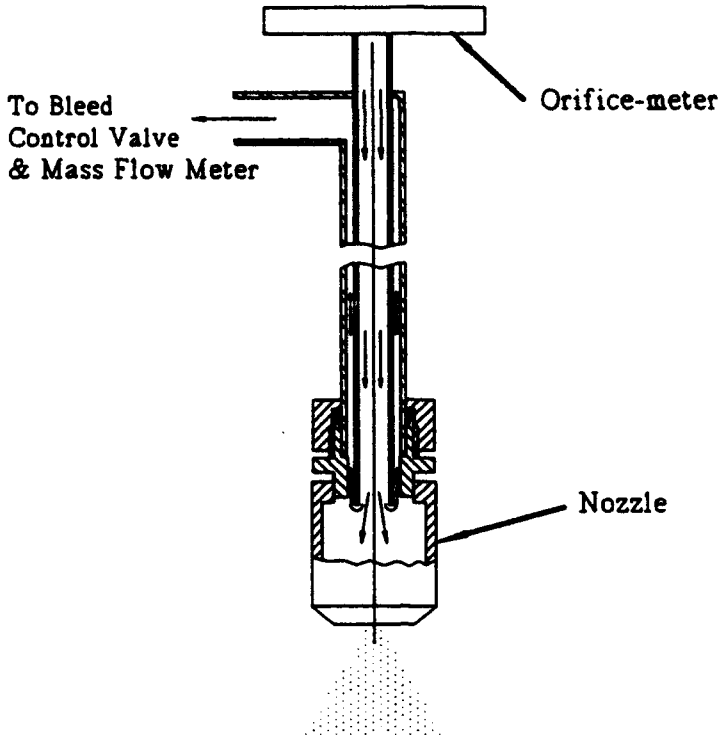

Figure 5.2 Bleed Port Details

the chamber is always maintained at atmospheric pressure, the liquid spraying out of the nozzle is always close to saturation if the upstream temperature is maintained at about 78 K (assuming isentropic expansion). All the lines are insulated with polyurethane foam to minimize heat gain. During preliminary experiments, it was found that, at low flow rates, it was very difficult to maintain a single phase fluid supply into the nozzle inlet, this resulted in violent pressure fluctuations and eventual disruption of flow. This happened because the heat gain into the line was sufficient to vaporize a part of the liquid flow at low flow rate. In order to overcome this problem, a bleed port was provided as shown in Figure 5.2. Thus, the total flow through the line could be maintained high enough to prevent vaporization. The bleed flow is measured by vaporizing the bleed flow and measuring the flow rate of gaseous nitrogen by a mass flow meter.

The heater, shown in Figure 5.3, is made out of oxygen free copper. The cartridge heater inserted inside the copper block provides the heat. The power to the cartridge heater is supplied by a variac. The heat transfer surface is a 1-cm^2 circle on the top of the block. The two

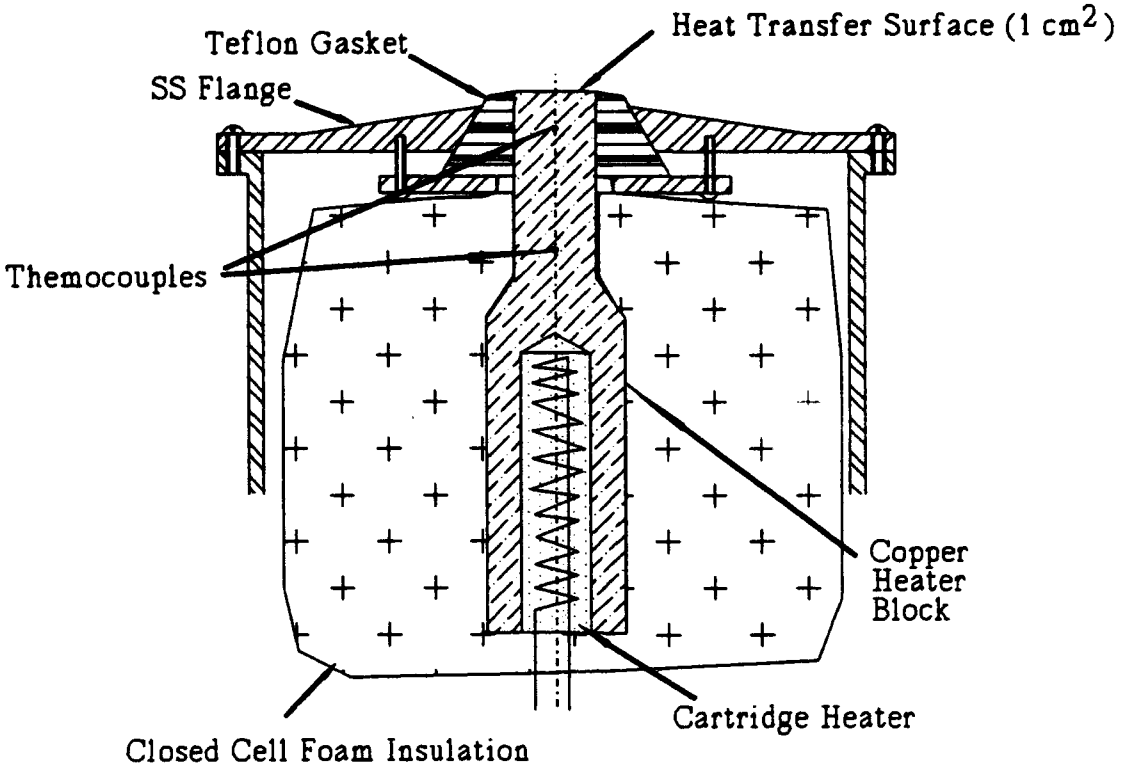

Figure 5.3 Heater Details

thermocouples in the copper block below the heat transfer surface are used to measure the temperature gradient below the surface. The heat flux and the surface temperature is estimated from these thermocouple measurements. All surfaces of the heater block except the top are insulated using polyurethane foam (k=0.035 W/m^2.K) to prevent heat loss. The heat loss from the block was estimated to be less than 2% with this insulation. The heat input from the cartridge heater is found by measuring the power input to the heater using a power transducer.

In addition to those in the copper block, thermocouples were also placed on the insulation surface, inside the chamber, on the nozzle body, instream near nozzle inlet, in the subcooling heat exchanger and on the chamber surface. The liquid flow rate to the nozzle is calculated by subtracting the bleed flow rate from the flow rate measured by the orifice-meter shown in Figure 5.1. All of the thermocouples and the power transducer output was read by a Fluke Helios Plus data acquisition system connected to a personal computer (Compaq 386/20e). During the experimental runs all data was recorded by the computer.

5.2 Experimental Procedure

An experimental run involves spraying the LN2 at a certain pressure and 78 K through the nozzle onto the heater surface. The roughness of the heater surface was measured before the heater was installed in the chamber, this roughness is not changed throughout the spectrum of experiments presented in this report. The surface was cleaned with a very dilute solution of hydrochloric acid and then rinsed with deionized distilled water and propanol prior to each set of experiments. Before beginning the experiment, the chamber is flushed with nitrogen to expel any air or water vapor. The subcooling heat exchanger shell is then filled with LN2 and the fluid is allowed to flow from the dewar to the nozzle. The bleed port is kept fully open till the line cools down to LN2 temperature. This is evidenced by the temperature of the nozzle reaching 78 K. The pressure of the dewar is now set at the desired value by venting the dewar or pressurizing it from a N2 gas cylinder. The bleed valve is then adjusted till the bleed flow is as low as possible while still sufficient to maintain the nozzle temperature at 78 K. The nozzle height and alignment is then adjusted to ensure that the spray covers the whole heat transfer surface and all the spray impinges the surface.

The power to the heater cartridge is then increased in steps of 5 W till dryout of the surface occurs. After each step increase in power, sufficient time is allowed for all the temperatures to reach steady state. The power to the heater is cut off immediately following the dry-out. Dry-out is evidenced by the rapid increase in temperature readings of the two thermocouples inside the copper block. Upon dry-out the temperature of the surface usually reaches approximately 200 K because of the thermal inertia of the heater block. The data recording is continued till the surface temperature falls back to about 80 K under the same spray conditions. Although these cooldown readings are not at steady state, the correct heat flux and surface temperature can be estimated by correcting for the temperature transients. The cooldown readings provide the heat transfer characteristics for LN2 spray cooling in the Leidenfrost point region.

In general, a set of runs were taken consecutively till the LN2 in the dewar ran out or the nozzle had to be changed. The set of results presented here involved four nozzles, TG0.3, TG0.5, TG0.7 and FLNo.13. The TG series nozzles are full cone pressure atomizing nozzles commercially available from Spraying Systems Co., Wheaton, IL. These nozzles have a flow swirler before the orifice which creates turbulent flow for effective atomization. The FLNo.13 is a flat disc shaped nozzle with radial grooves leading to the orifice (for creating turbulence).

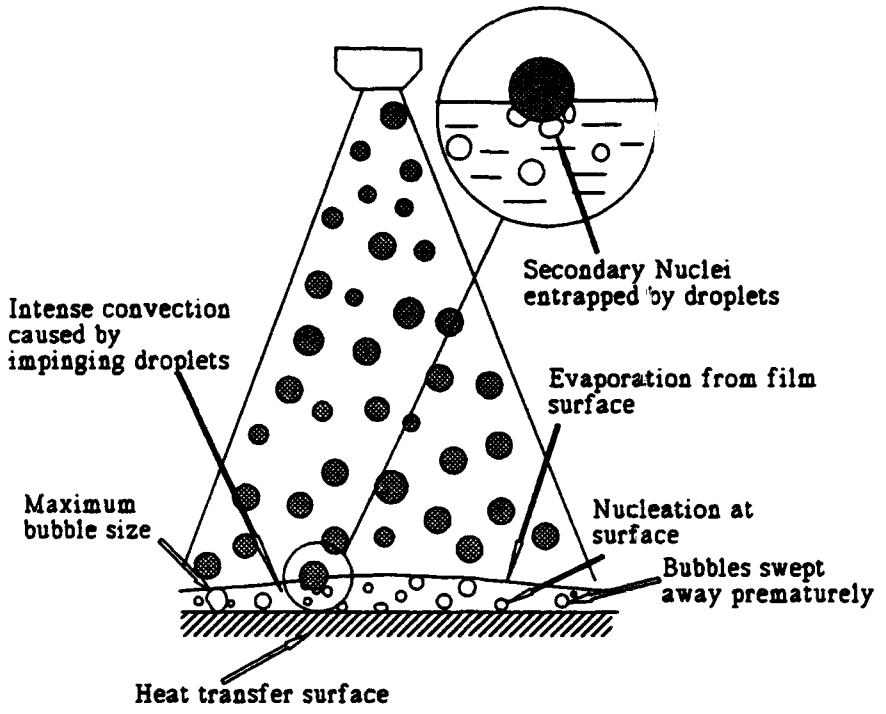

Figure 5.4 Spray Cooling

The orifice diameter for these nozzles is given in Table 5.1.

Table 5.1

Nozzle	Orifice Diameter
TG0.3	0.51 mm
TG0.5	0.61 mm
TG0.7	0.76 mm
FLNo.13	0.38 mm

The experiments were carried out for five to six different pressures for each nozzle (30, 40, 60, 80, 100, and 120 PSIG). The nozzle inlet pressure was continuously monitored by a Bourdon gauge connected to the low pressure side of the orifice-meter. The spray cone for the FLNo.13 nozzle (about 30°) was much narrower than that for TG series nozzles (about 60°).

The nozzle height above the surface was varied to keep the surface covered with spray, all the experiments with TG series nozzles had approximately the same nozzle height, 1 cm; the height for FLNo.13 nozzle was 2 cm.

5.3 Results and Discussion

A brief discussion of spray cooling theory will provide a better insight into the results presented here. Figure 5.4 shows the probable mechanisms involved in spray cooling heat transfer. Convection heat transfer, evaporation from the film surface, nucleate boiling at the heater surface and secondary nucleation are all thought to be involved in spray cooling. The intense convection caused by impinging droplets enhances the heat transfer between the heater surface and the free surface of liquid film, the heat transferred to the film surface goes towards evaporation of the fluid. Nucleate boiling at the heater surface also helps in increasing the heat transfer coefficient greatly. And finally, secondary nucleation, which results from the entrapment of vapor bubbles by impinging droplets, may also play a very important role in spray cooling [17]. The relative importance of each of these heat transfer mechanisms is unknown to date, but inspite of the lack of that information, the hypothesis provides a useful tool for evaluating the experimental results. Also, the experimental data will help in resolving the various issues involved in the hypothesis.

The results for each nozzle are presented first, and then comparisons are made based on the mass flow rate and nozzle type. All the TG series nozzles show some degree of nonuniformity in spray; the spray cone is usually less dense along the axis compared to the edge. The implications of this nonuniformity will be discussed.

5.3.1 Individual Nozzle Results

The TG0.3 had the smallest orifice of all the TG series nozzles used in this study. The spray for this nozzle was very dense and slightly hollow along the axis. Figure 5.5 shows the superheat (T_w-T_{sat}) vs. heat flux data for three different flow rates (or nozzle pressures). In the figure, the heat transfer curve is made up of three distinct regions. The first is the low superheat region, here, the heat transfer is probably dominated by forced convection with evaporation from the film surface, and secondary nucleation.

Nucleate boiling at the surface is absent in the first region because surface nucleation

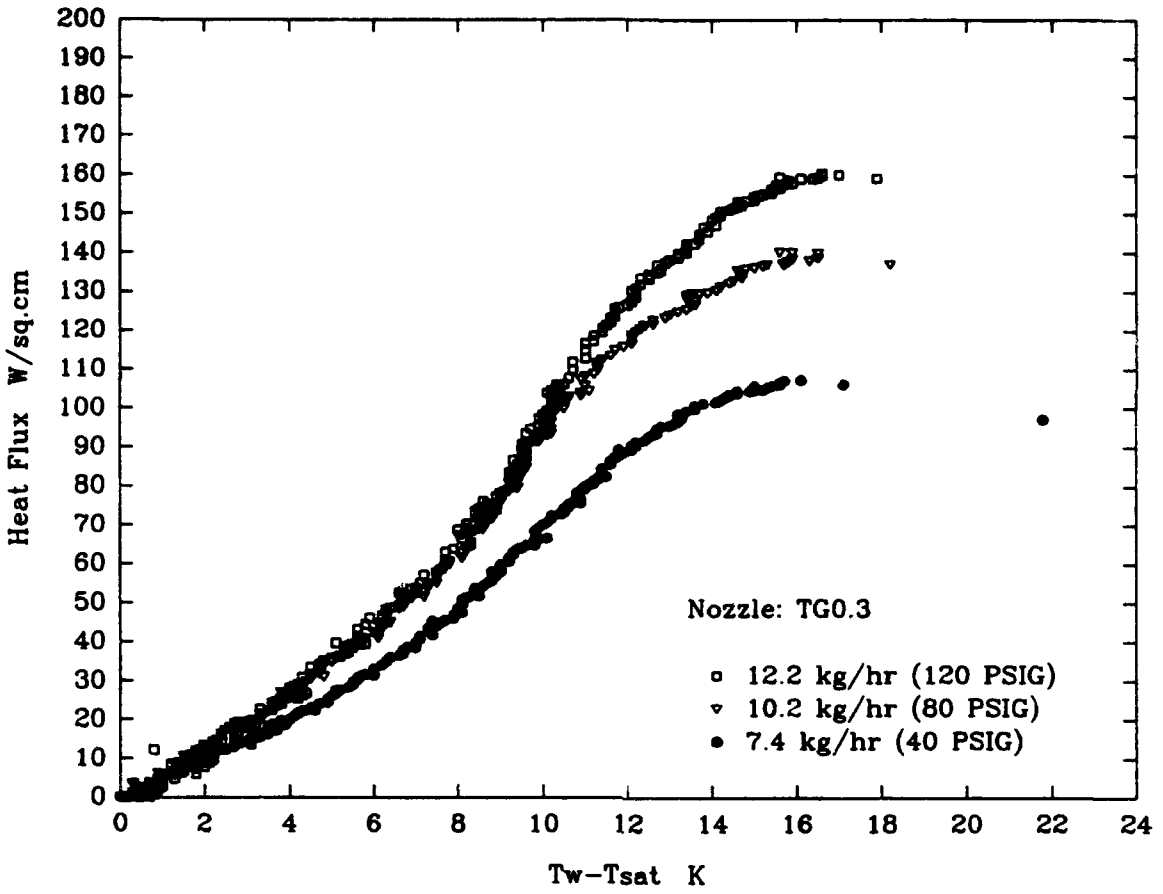

Figure 5.5 TG0.3 Heat Transfer Characteristics

usually begins at a higher superheat in forced convection situations and is noticeable by a distinct change in slope [18]. As the superheat is increased, the slopes of the curves show a small jump at about 9 K superheat, this is probably due to the beginning of nucleate boiling on the heater surface.

Once the nucleate boiling on the heater surface has begun, the curves in Figure 5.5 show a definite shift upwards, this second region can be said to have a significant contribution by surface nucleation. Upon reaching a superheat of about 15 K, the curves in Figure 5.5 become almost horizontal, this is due to the partial dry-out of the surface. As mentioned earlier, the spray is slightly hollow along the axis, hence, the dryout starts on the center of the surface (due to lower mass flux at the center) and progresses outward. This shows up as a gradual increase in average surface temperature with almost no increase in heat flux. When the surface is fully dry, the heat input is cut off, the surface temperature goes to a higher value because of the thermal inertia of the copper block. The block then begins to cool down under Leidenfrost

conditions, the heat flux under these conditions is around 20-30 W for the cases shown in Figure 5.5. The heat flux reaches a minimum value at around 45 K superheat and then starts rising rapidly as the droplets begin to wet the surface.

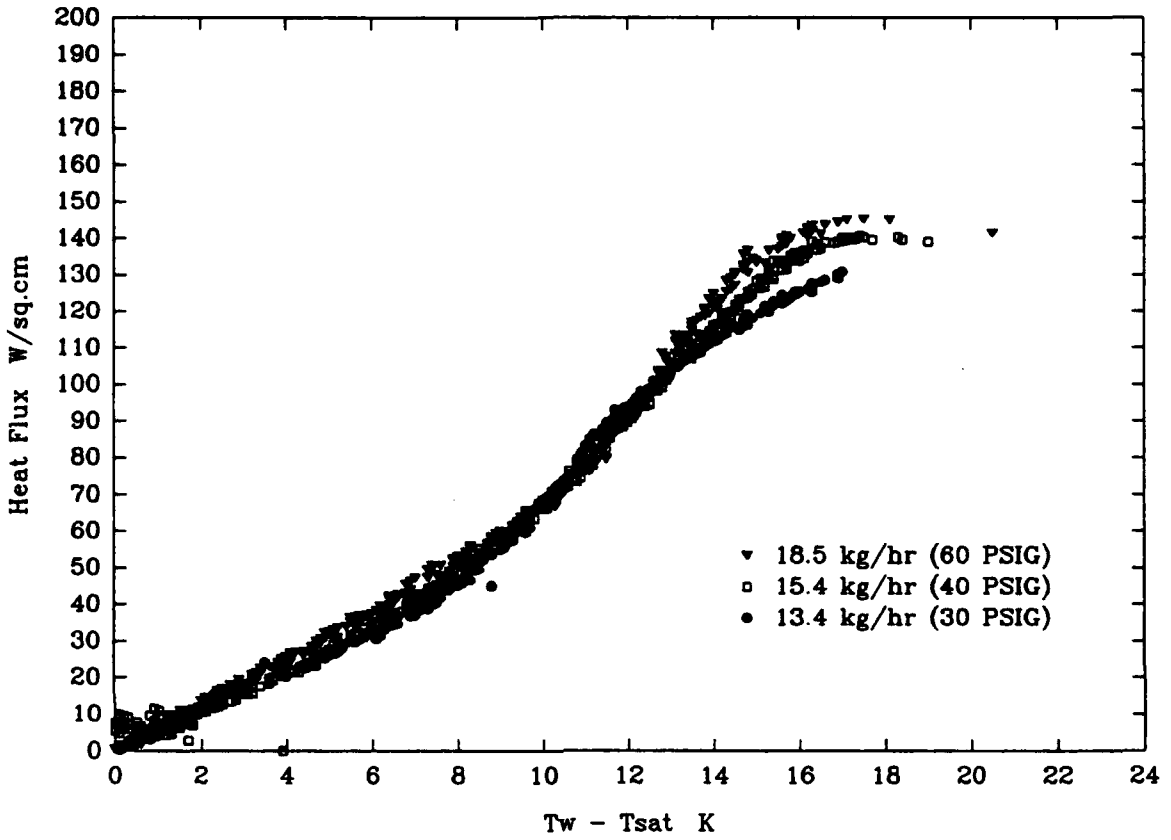

Figure 5.6 TG0.5 Heat Transfer Characteristics

The influence of mass flow rate on heat transfer characteristics is quite clear from Figure 5.5, the critical heat flux (CHF) and heat transfer coefficient show an increase with increase in mass flow rate. This effect is more pronounced for CHF, where a more significant increase is seen with increase in flow rate.

Figure 5.6 shows the heat transfer characteristics for spray cooling with the TG0.5 nozzle. The trends are similar to those described for the TG0.3 nozzle. The increase of mass flow rate leads to an increase in heat transfer coefficient and CHF. The spray from this nozzle was a little less hollower than TG0.3, this results in a shorter third region.

The spray from the TG0.7 nozzle was very dense and slightly hollow in the middle. Figure 5.7 shows the heat transfer characteristics for this nozzle. The trends in the curves and mass flow rate effect are similar to the previous cases.

Figure 5.8 shows the heat transfer characteristics for the FLNo.13 nozzle. This nozzle had

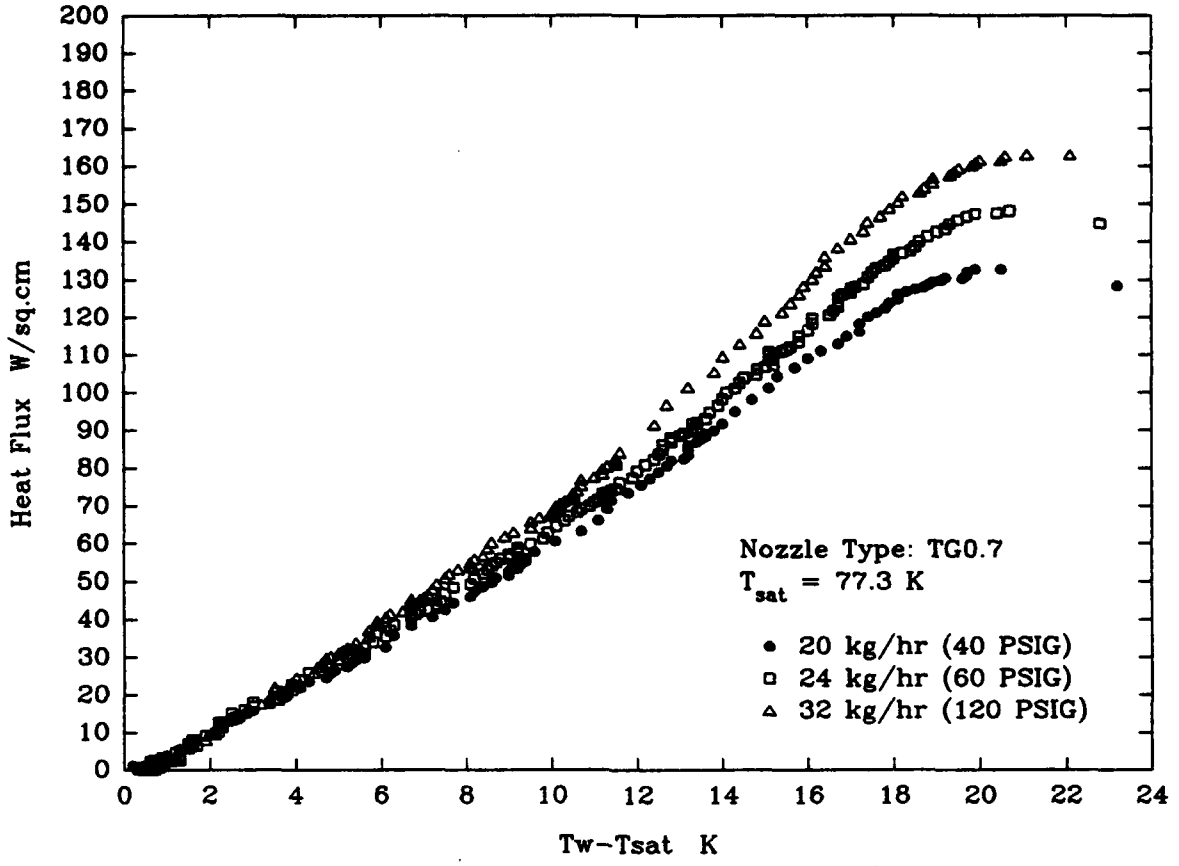

Figure 5.7 TG0.7 Heat Transfer Characteristics

the smallest orifice diameter, and hence, the lowest flow rate at any particular pressure. The spray from this nozzle was very well distributed and the nonuniformity was not noticeable from a visual observation. In Figure 5.8, the different flow rate curves for this nozzle are more distinguishable from each other compared to the other cases. The increase in heat transfer coefficient and CHF with increase in mass flow rate is clearly evident.

5.3.2 Comparison of Nozzles

Since the effect of flow rate on CHF is most pronounced, the CHF vs. mass flow rate characteristics for different nozzles are compared first. This comparison is shown in Figure 5.9. As is clearly evident from the figure, all nozzles show an increase in CHF with increase in mass flow rate. However, the increase in nonlinear, i.e., there is a diminishing increase in CHF with increase in mass flow rate. This means that CHF is a power function of mass flow rate as in Equation 5.1:

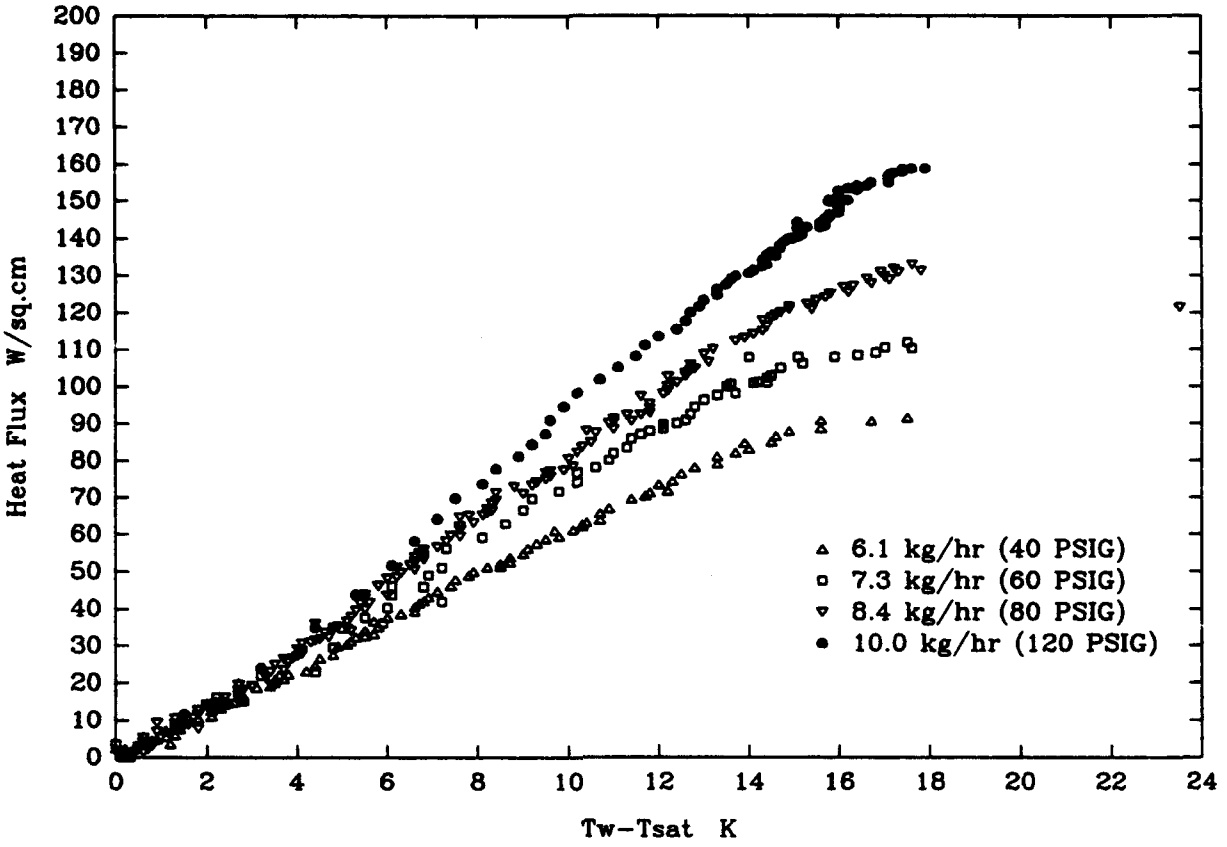

Figure 5.8 FLNo.13 Heat Transfer Characteristics

$$CHF = \alpha \dot{m}^n \qquad \text{(Equation 5.1)}$$

The values of α and n based on the data shown in Figure 5.9 are tabulated in Table 5.2. The

Table 5.2

Nozzle Type	α	n
TG0.7	1617.7	0.48
TG0.5	1155.4	0.39
TG0.3	14943.1	0.80
FLNo.13	56160.0	1.00

table shows that α and n are not the same for all nozzles, hence, it can be safely concluded that α and n are functions of spray characteristics and possibly of surface roughness as well.

From looking at Figure 5.9, it is apparent that the efficiency of spray cooling increases as the nozzle size is decreased. Here, efficiency ϵ is defined as:

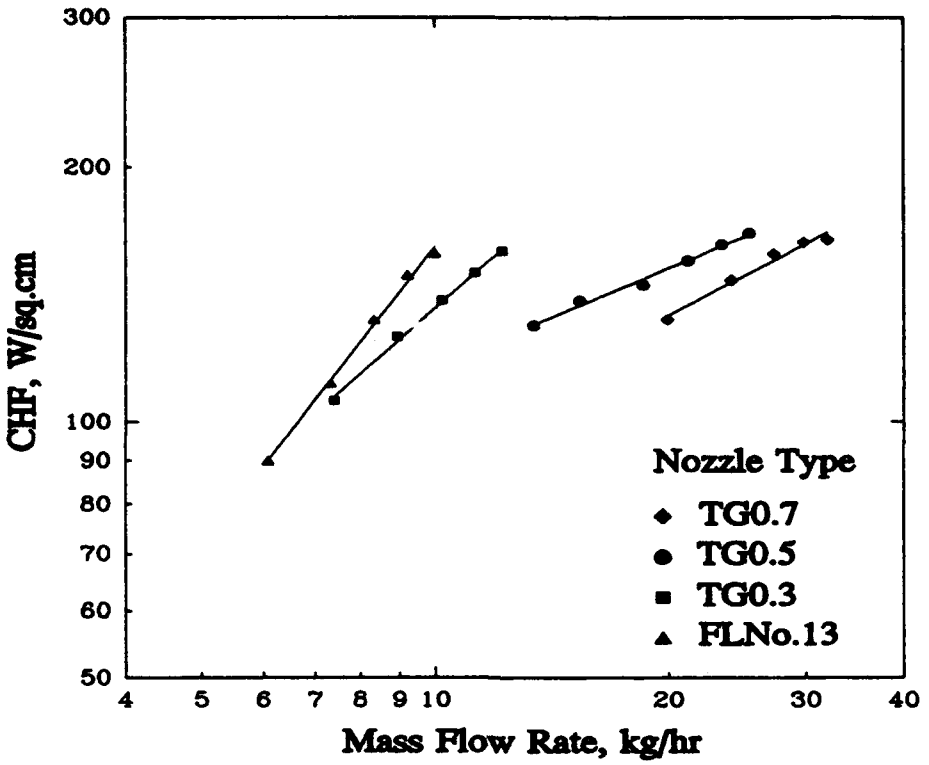

Figure 5.9 Effect of Nozzle and Mass Flow Rate on CHF

$$\epsilon = \frac{CHF}{\dot{m} h_{fg} / A_{surf}} \qquad \text{(Equation 5.2)}$$

Figure 5.10 shows the efficiency vs. flow rate characteristics of all the nozzles used in this study. The higher efficiency of smaller nozzles is probably due to all or some of the following reasons:

a) The flow rate obviously decreases with nozzle size, this leads to thinner liquid film with decrease in nozzle size. The thinner liquid film results in lesser thermal resistance to heat transfer from the heater surface to the free surface of liquid film, this in turn leads to more evaporation from the film surface.

b) The velocity of the droplets usually increases with decrease in nozzle size [19], this leads to higher convection heat transfer.

c) The number of droplets per unit area per unit time increases with decrease in nozzle size [19,20]. This would probably result in an increase in secondary nucleation and convection in the liquid film.

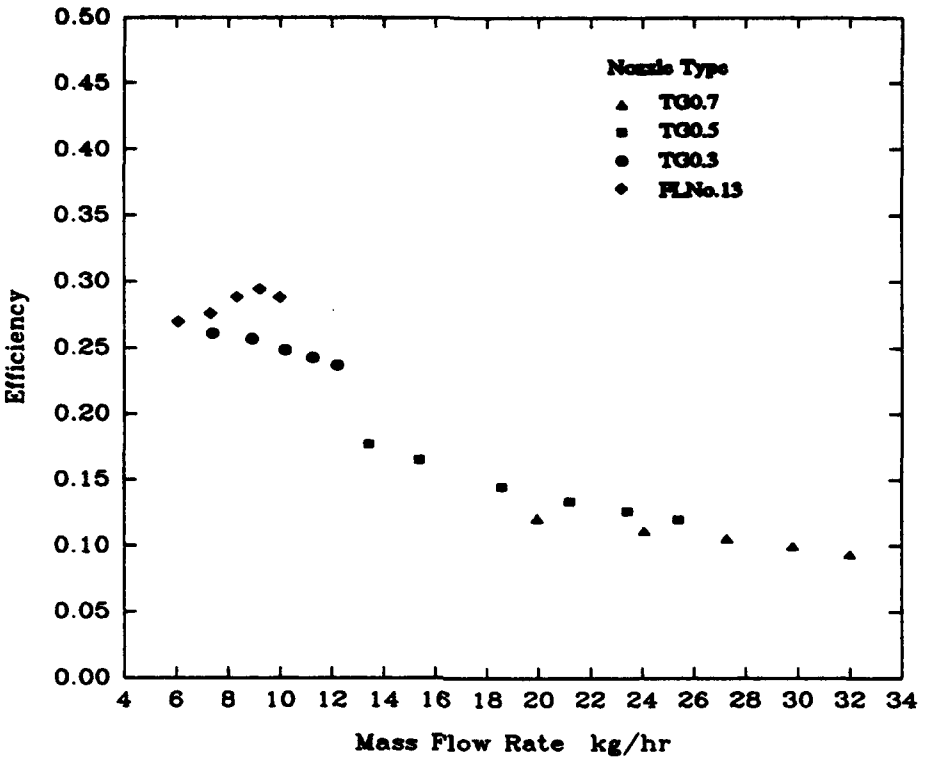

Figure 5.10 Effect of Nozzle on Efficiency

The effects mentioned above cannot be quantified till the spray characteristics have been measured.

The comparison of heat transfer characteristics for any two nozzles is more valid if the mass flow rates are the same, this eliminates the film thickness effect from consideration. Figure 5.11 shows a comparison of TG0.5 and TG0.3 nozzle at a flow rate of about 12 kg/hr. The heat transfer coefficient and CHF is higher for the TG0.3 nozzle, this clearly shows the effect of spray parameters on heat transfer characteristics and points to the need of measuring them. The effect of surface parameters also needs to be investigated before a comprehensive correlation can be formulated.

The effect of flow rate and nozzle type on the heat transfer in Leidenfrost region was also investigated. Figure 5.12 shows the results. The minimum heat flux in the Leidenfrost region occurs just before the droplets begin to wet the surface. The figure shows that the minimum heat flux increases with the mass flow rate for any nozzle. The momentum of the droplets is the most important parameter in the Leidenfrost region. The higher momentum droplets can get closer to the surface and, thus, enable higher heat transfer at the surface. The average droplet size increases as the nozzle size increases (at same nozzle pressure) [19]. Hence, the larger nozzles

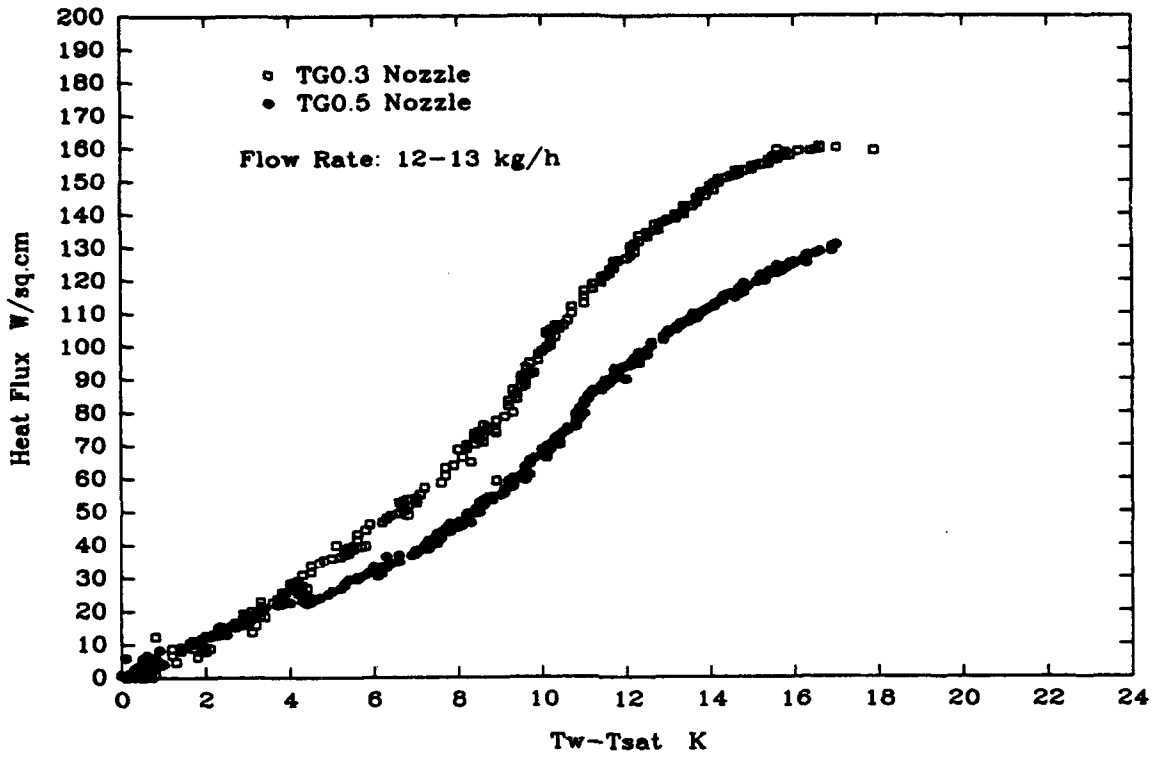

Figure 5.11 Comparison of Heat Transfer Characteristics

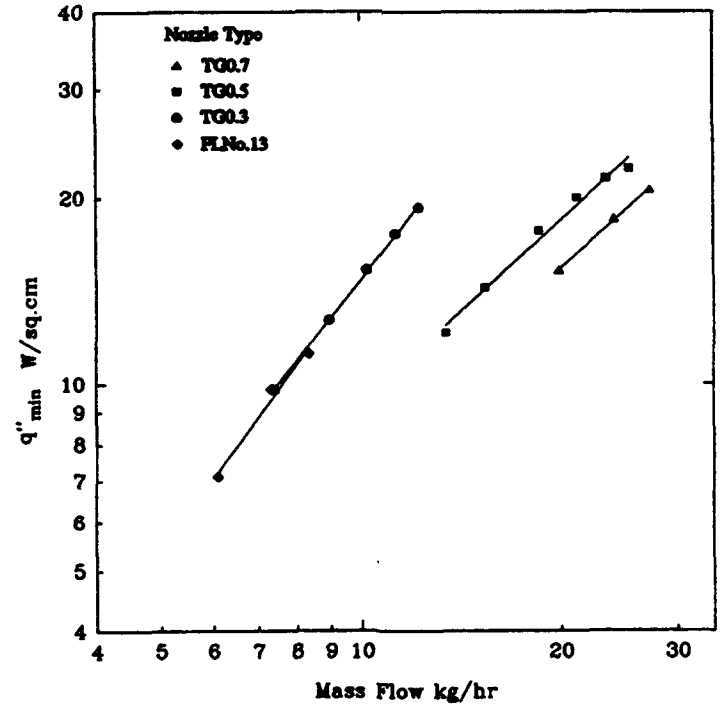

Figure 5.12 Effect of Flow Rate and Nozzle on Minimum Heat Flux

produce sprays which have droplets with higher momentum. Therefore, the larger nozzles

perform a little better in the Leidenfrost region.

6. POOL BOILING HEAT TRANSFER FROM DISCRETE SOURCES IN CONFINED SPACE

Of all the different methods of heat removal, pool boiling, which occurs when a stationary liquid cools a heat sink, is the least complicated. Though incapable of removing the high quantities of heat that spray cooling and flow boiling can, pool boiling is simple, effective, and relatively inexpensive. This makes it an attractive option in cooling situations where heat removal requirements are not very large.

One field in which pool boiling has practical applications is electronic cooling. The numerous benefits of operating electronics at low temperatures have been pointed out by various researchers: circuits operate faster, semiconductors switch more rapidly, heat removal capacities increase, the number of thermally-induced device failures decrease, and the noise-to-signal ratios drop [21-24]. These advantages are usually associated with temperatures between 10 and 100 K, when the thermal and electrical conductivities of common circuit materials, such as copper and silicon, are maximized [25]. One inexpensive coolant whose vaporization point, 77.3 K, falls into this temperature range is liquid nitrogen (LN2).

A reliable method which could maintain liquid nitrogen temperature (LNT) in circuits would be of vast importance to the electronics industry. Operating electronics at LNT is very advantageous. As decreasing the size of integrated circuits becomes more difficult and more expensive, it has been predicted by some observers that low temperature electronics will become a very attractive option [26]. In fact, they believe that operation at LNT can improve circuit performance more than decreasing their size by a factor of 2.

Though extensive studies have been conducted on pool boiling, they have mostly been done on conventional, open-area boiling. However, the situation in most electronic equipment, as well as in most heat transfer equipment, is a series of confined areas where bubbles from several discrete heat sinks may interfere with each other or may be deformed. Very little is known about how confinement affects pool boiling, and even less is known about its effect on cryogens, such as liquid nitrogen. Previous experiments that have been conducted on confined

pool boiling have used conventional liquids, such as water [27,28], acetone [27], fluorocarbons [29,30], or Freon [27]. Very little research has been done using LN2, Reference [31] reports a study of two chips facing each other, with a very small gap, suspended in a pool of LN2. The purpose of this experiment is to study the change in critical heat flux (CHF) of LN2 as the gap between a heater and an opposing glass plate decreases. In addition, the effect of neighboring heat sources on CHF will also be studied.

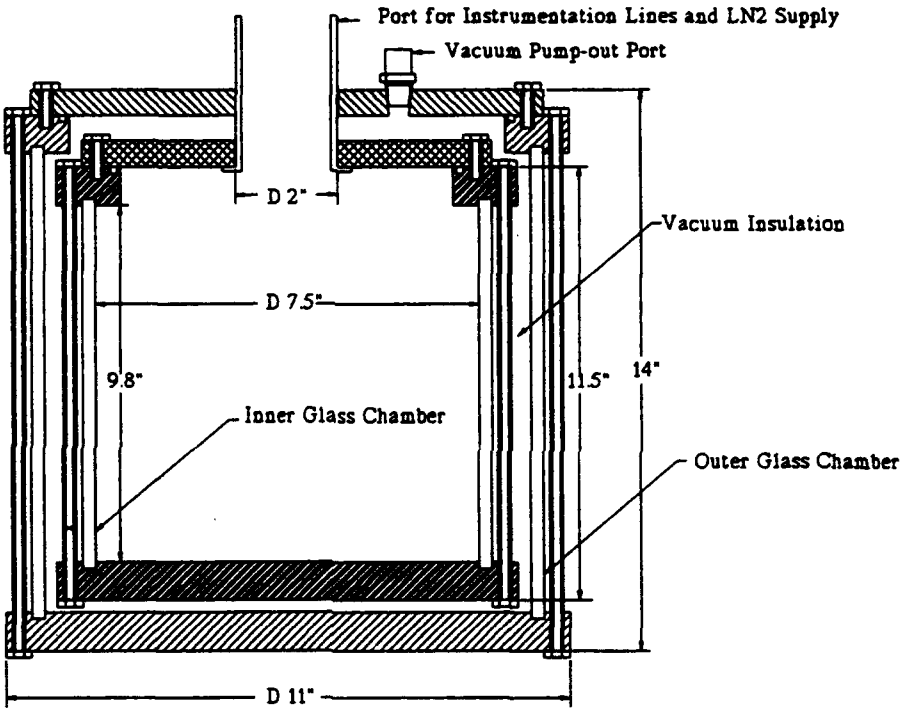

Figure 6.1 Experiment Chamber

6.1 Experimental Design

Experiments are conducted in a seamless glass cylinder with an inner diameter of 7.50 inches, an outer diameter of 8.00 inches, and a height of 10 inches (Figure 6.1). It will contain a pool of LN2 during the experiment. To prevent heat transfer from the environment, this cylinder is placed inside another glass tube with inner diameter 9.45 inches. The space between the two cylinders is insulated by a pump-maintained vacuum. This allows the experiments to be observed and videotaped.

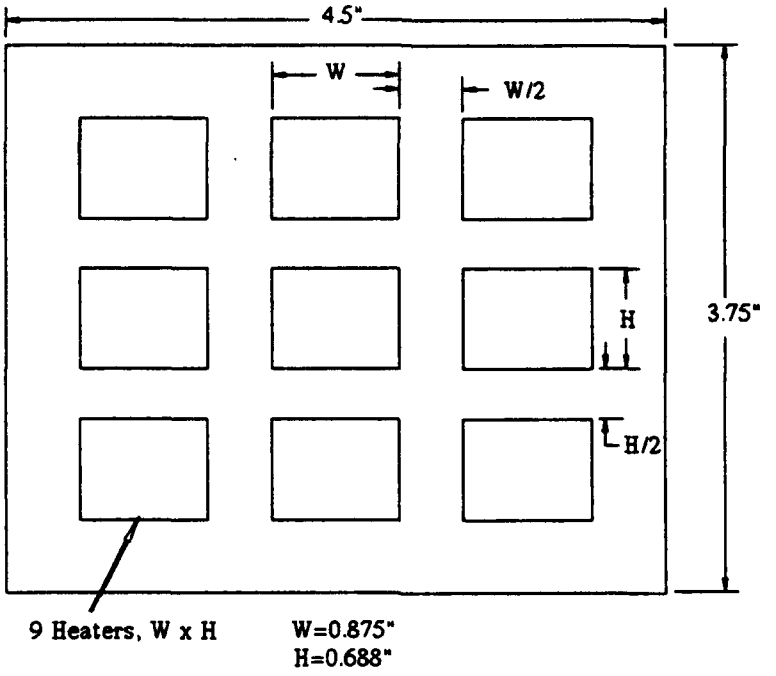

Figure 6.2 Heater Arrangement

Nine electrically-powered heaters (0.875 inches by 0.688 inches) on copper blocks are

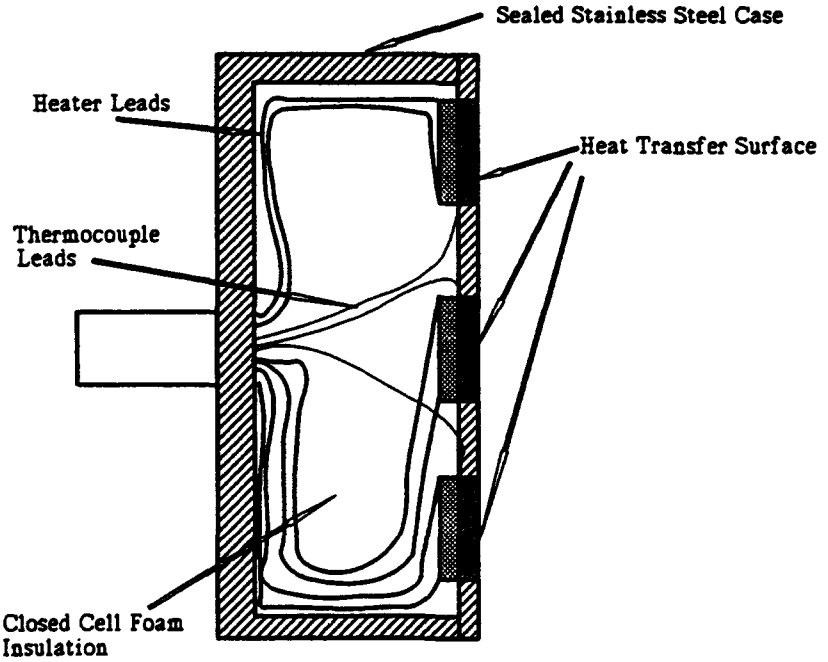

Figure 6.3 Heater Case

mounted flush with a stainless steel sheet 4.50 inches long, 3.75 inches wide, and 0.10 inches thick (Figure 6.2). Temperatures in the heaters are monitored by type E thermocouples. The plate is screwed to a stainless steel case which shields the electric wiring and thermocouple wires from the LN2. A stainless-steel spacer separates the heaters from a glass plate, which confines the boiling to the gap between it and the heaters. The entire assembly is fixed to a base to keep it from moving during experiments and placed within the inner glass cylinder. Figure 6.3 shows the schematic diagram of the heater box. All data, such as heater temperature and power dissipation, is collected by IBM PC 386 through a programmed Hewlett Packard 3852A Data Acquisition/Control Unit equipped with a 5-1/2 digit voltmeter and a 20 channel relay multiplexer. Figure 6.4 shows the data acquisition and electrical circuit arrangement for one of the nine heaters.

6.2 Experiment Procedure

The experimental set-up has been completed and the experiments are in progress at the present time. Experiments will be conducted with different spacings in front of the heaters and

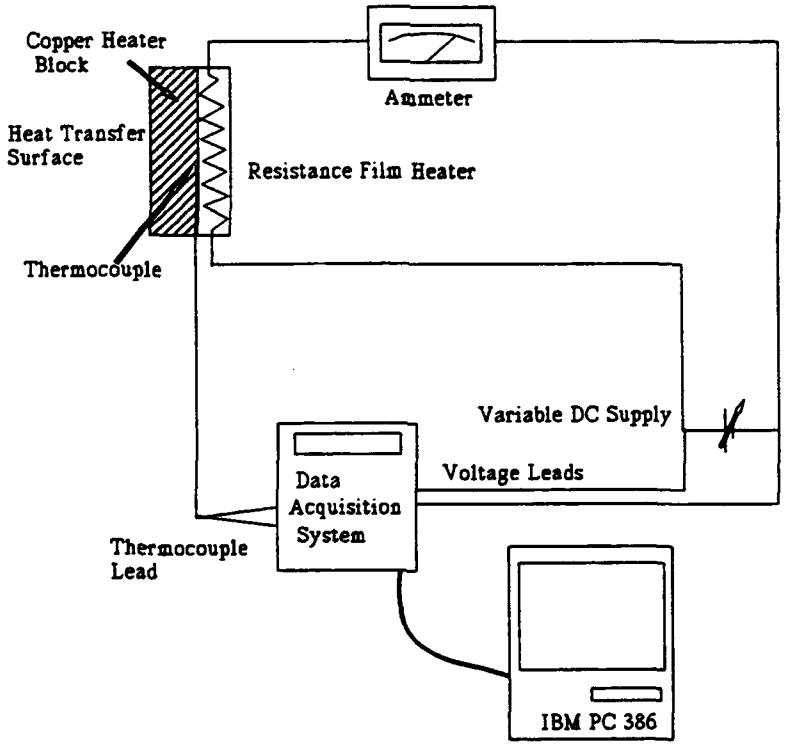

Figure 6.4 Data Acquisition and Electrical Circuit

various different heat flux distributions. During an experiment, heat flux to one of the nine heaters will be varied and its heat transfer characteristics examined while the other eight heaters are maintained at some fixed heat flux level. This way heat transfer characteristics at each position on the heater plate will be determined at different environmental conditions (i.e., varying bubble generation from the surrounding heaters).

7. CONCLUSIONS AND FUTURE PLANS

The free expansion (blow-down) of liquid and supercritical nitrogen was studied at different upstream pressures, downstream pressures and three different nozzle sizes. It was found that the nozzle size and geometry had a great influence on the process. For downstream pressures below triple point, nitrogen exiting the nozzle generally solidified irrespective of the upstream pressure. Solid nitrogen formed before nozzle exit for the smallest nozzle because of flow throttling, this resulted in slow oozing out of solid nitrogen from this nozzle. The other two nozzles sprayed out droplets of nitrogen which solidified in the vacuum chamber and then accreted on the thermocouples which were in the spray trail. The mass flow rates and the cooling speed for the three nozzles were also measured.

Spray cooling with liquid nitrogen was carried out for four different nozzle sizes and two nozzle types. It was found that the heat transfer coefficient and CHF are strong functions of spray characteristics and possibly surface characteristics. CHFs up to 170 W/sq.cm were observed, CHF generally occurred at around 95 K. The efficiency of spray cooling ranged from 8% for the TG0.7 nozzle to 30% for the FLNo.13 nozzle. The spray characteristics are currently being measured and the effect of surface roughness will be studied soon.

The experimental set-up for the pool boiling in confined space study has been completed and the experiments are currently in progress. Experiments will be carried out for various heat flux distributions and spacings.

8. REFERENCES

1 Nisenhoff, M., "Superconducting electronics: current status and future prospects," *Cryogenics*, Vol. 28, No. 1, pp. 47-56, 1988.

2 Van Duzer, T., "Superconductor-semiconductor hybrid devices, circuits and systems," *Cryogenics*, Vol. 28, No. 8, pp.527-531, 1988.

3 Van Duzer, T., "Josephson digital devices and circuits," *IEEE Trans. on Microwave Theory and Techniques*, Vol. MTT-28, pp. 490-500, 1980.

4 Tucker, J.R., "Quantum limited detection in tunnel junction mixers," *IEEE J. of Quantum Electronics*, QE-15, pp. 1234-1258, 1979.

5 McGrath, W.R., Raisanen, A.V., Richards, P.L., Harris, R.E. and Lloyd, F.L, "Accurate noise measurements of superconducting quasiparticle array mixers," *IEEE Trans. on Magnetics*, Vol MAG-21, pp. 212-221, 1985.

6 Clarke, J., "Superconducting quantum interference devices for low frequency measurements, superconducting applications," *SQUIDs and Machines*, Editors: Schwartz, B.R. and Foner, S., Plenum Press, NY, Ch. 3, pp. 67-124, 1977.

7 Silver, A.H. and Zimmerman, J.E., "Quantum states and transition in weakly connected superconducting rings," *Physics Review*, Vol. 157, pp. 317-341, 1967.

8 Flik, M.I and Hijikata, K., "Approximate thermal packaging limit for hybrid superconductor-semiconductor electronic circuits," Proc. Ninth Int. Heat Transfer Conf., Jerusalem, Israel, Vol. 2, pp. 319-324, 1990.

9 Lavine, A.S. and Bai, C., "An analysis of heat transfer in Josephson junction devices," *J. of Heat Transfer*, Vol. 113, pp. 535-543, 1991.

10 Van Duzer, T., "Superconductor electronic device application," *IEEE J. of Quantum Electronics*, Vol. QE-25, No. 11, pp. 2365-2377, 1989.

11 Fox R.M. and Jaeger R.C., "MOSFET behavior and circuit considerations for analog applications at 77 K," *IEEE Trans. on Electron Devices*, Special Issue on Low Temperature Semiconductor Electronics, Vol. ED-34, No. 1,pp. 114-123, 1987.

12 Mueller, O., "Cryogenic power conversion: combining HT superconductors and semiconductors," AIP Conf. proceedings 251, pp. 746-759, 1991.

13 Touloukian, Y.S., Powell, R.W, Ho, C.Y. and Clemens P.G., *Thermophysical Properties of Matter The TPRC Data Series*, Vol. 1 & 2, IFI/Plenum, NY, 1970.

14 Chow, L.C., Sehmbey, M.S., Pais, M.R., Lu, W.F. and Hahn, O.J., "Fundamental Studies in Hydrogen Blowdown and Cryogenic Cooling," UK-ME-92-06, Interim Report for September 1991- August 1992, 1992.

15 Pais, M.R., "Determination of the Local Heat Transfer Characteristics on Glaze-ice accretions on a Cylinder and a NACA 0012 Airfoil," Ph.D. Dissertation, University of Kentucky, 1987.

16 Gayle, J.B., Egger, C.T., Bransford, J.W., "Freezing of Liquids on Sudden Exposure to Vacuum," *J. of Spacecraft*, Vol.1, No. 3, 1964.

17 Mesler, R. and Bellows, W.S., "Explosive Boiling: A Chain Reaction Involving Secondary Nucleation," ASME Proc.of 1988 National Heat Transfer Conference, HTD-96, Vol.2 , pp. 246-252, 1976.

18 Rosenhow, W.M., Hartnett, J.P. and Ganić, E.N., Editors, *Handbook of Heat Transfer Fundamentals*, 2nd. Ed., McGraw Hill, Inc., NY, 1985.

19 Lefebvre, A.H., *Atomization and Sprays*, Hemisphere Pub. Corp., NY, 1989.

20 Tilton, D.E., "Spray Cooling," Ph.D. Dissertation, University of Kentucky, 1989.

21 Gaensslen, F.H., "MOS devices and Integrated Circuits at Liquid Nitrogen Temperature," *1980 IEEE ICCD Proceedings*, pp. 450-452, 1980.

22 Kirschman, R.K., "Cold Electronics: An Overview," *Cryogenics*, Vol. 25, pp. 115-122, 1985.

23 Kirschman, R.K., *Low Temperature Electronics*, IEEE Press, NY, 1986.

24 Jaeger, R.C., "Development of Low Temperature CMOS for High Performance Computer Systems," IEEE Int. Conf. of Computer Design: VLSI in Computers, pp. 128-130, 1986.

25 Krane, R.J., Bar-Cohen, A., Jaeger, R.C. and Gaensslen, F.H., "MOS Electronics and Thermal Control for Cryogenically-Cooled Computer Systems," *Advances in Thermal Modeling of Electronic Components and Systems*, Vol. 2., Editors: Avram Bar-Cohen and Allan D. Kraus, ASME Press, NY, 1990.

26 Jaeger, R.C. and Gaensslen, F.H., "Low Temperature Semiconductor Electronics," Proceedings of Thermal Phenomena in Electronic Components, I-THERM 1988 Conf., LA, pp. 106-114, 1988.

27 Yao, S. and Chang, Y., "Pool Boiling Heat Transfer in a Confined Space," *Int. J. of Heat Mass Transfer*, Vol. 26, No. 6, pp. 841-848, 1983.

28 Fujita, Y., H. Ohta, S. Uchida, and K. Nishikawa. "Nucleate Boiling Heat Transfer and Critical Heat Flux in Narrow Space Between Rectangular Surfaces," *Int. J. of Heat Mass Transfer*, Vol. 31, No. 2, pp. 229-239, 1988.

29 Mudawar, I. and Anderson, T.M., "High Flux Electronic Cooling by Means of Pool Boiling - Part I: Parametric Investigation of the Effects of Coolant Variation, Pressurization, Subcooling, and Surface Augmentation." 1989 National Heat Transfer Conf., Heat Transfer Division, Vol. 111, Heat Transfer in Electronics, pp. 25-34, 1989.

30 Mudawar, I. and Anderson, T.M., "High Flux Electronic Cooling by Means of Pool Boiling - Part II: Optimization of Enhanced Surface Geometry." 1989 National Heat Transfer Conf., Heat Transfer Division, Vol. 111, Heat Transfer in Electronics, pp. 35-49, 1989.

31 Tuzla, K., Çökmez-Tuzla, A.F., Crowley, A.J. and Chen, J.C., "Cooling of Electronic Chips in Liquid Nitrogen," Proceedings of the Ninth Int. Heat Transfer Conf., Jerusalem, Israel, Heat Transfer, Vol. 2, Editor: G. Hetsroni. pp. 301-306, 1990.

APPENDIX

Error analysis for spray cooling and free expansion studies are presented below. Additional data from the free expansion study is also included.

A.1 Error Analysis: Spray Cooling

The thermocouples used in the experiment were made from special grade E-type thermocouple wire manufactured by Omega, CT. The thermocouples were tested by immersing the bead in LN2 at atmospheric pressure (temperature 77.3 K), the temperatures ranged from 77.0 K to 78.0 K, hence, the error in absolute temperature measurement can be considered to be ± 0.7 K. The two thermocouples installed in the copper block were always within 0.3 K of each other during calibration, hence, the error in temperature difference used to estimate the heat flux is ± 0.3 K. Since the thermal conductivity of copper is not constant in the range of temperatures during the experiments, a piecewise polynomial interpolation was used to determine thermal conductivity, the error in thermal conductivity is 2 % according to [13]. The heat flux and surface temperature were calculated by a computer program which corrects for the variation in thermal conductivity with temperature. The uncertainties in estimated heat flux and surface temperature are given by:

$$\frac{\delta q''}{q''} = \left[\left(\frac{\delta k}{k}\right)^2 + \left(\frac{\delta \Delta T}{\Delta T}\right)^2 + \left(\frac{\delta l}{l}\right)^2\right]^{0.5} \qquad \text{(Equation A.1)}$$

$$\frac{\delta T_{surf}}{T_{surf}} = \left[\left(\frac{\delta q''}{q''}\right)^2 + \left(\frac{\delta k}{k}\right)^2 + \left(\frac{\delta l_2}{l_2}\right)^2 + \left(\frac{\delta T_2}{T_2}\right)^2\right]^{0.5} \qquad \text{(Equation A.2)}$$

Substituting the values of uncertainties in length, conductivity, temperature, and temperature difference gives the uncertainty in heat flux as 4% at 30 W. The uncertainty in heat flux decreases as the temperature difference between the two thermocouples increases, hence, the estimate increases in accuracy as the heat flux increases. Similarly, the uncertainty in surface

temperature estimate is 4.5% at 30 W and varies just like the heat flux.

As mentioned in Chapter 5, the mass flow rate is estimated by subtracting the bleed flow rate from the mass flow rate measured by the orifice-meter. Thus, the uncertainty in mass flow rate is estimated by combining the uncertainties in: differential pressure reading, orifice-meter discharge coefficient estimate, orifice diameter and bleed flow rate. The resulting uncertainty in mass flow rate was about 5%.

A.2 Error Analysis for Free Expansion

The vacuum gauge (transducer) used in the experiment had an accuracy of $\pm 3\%$ of the reading. The thermocouples after calibration had an accuracy of ± 1 K in the range of temperatures covered in this study. The mass flow rate uncertainty is based on the uncertainty in the stop watch reading and the final pressure reading. Based on these, the uncertainty in mass flow rate was $\pm 5\%$.

A.3 Free Expansion Study- Additional Data and Photographs

The following pages contain data and photographs not included in the main part of the report.

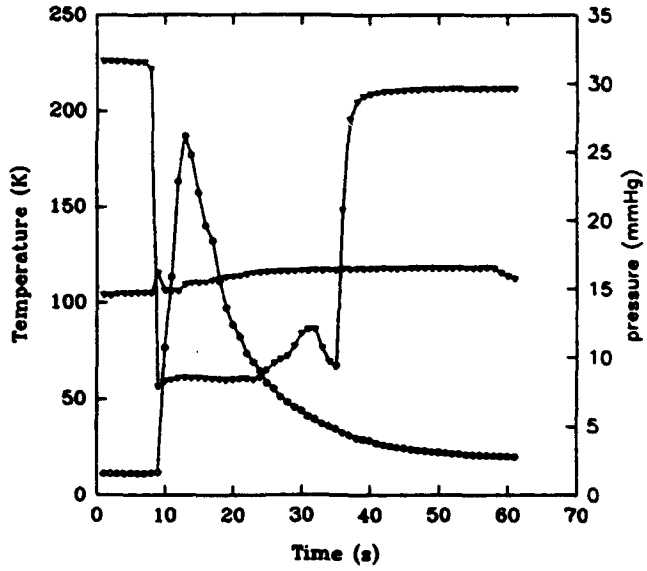

• –pressure
• –tmperature
nozzle d= 0.007"
upstream pressure: 200 psig
1–first thermocouple
2–temperature in injector

Figure A.1 Temperature and Pressure in Blow-Down Tube

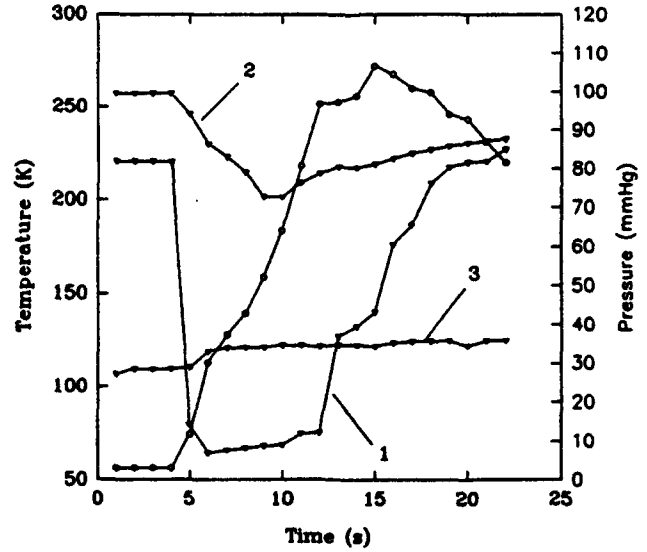

• –pressure
• –temperature
nozzle: d=0.007"
upstream pressure: 400psig
1--first thermocouple
2--second thermocouple
3--temperature in injector

Figure A.2 Temperature and Pressure in Blow-Down Tube

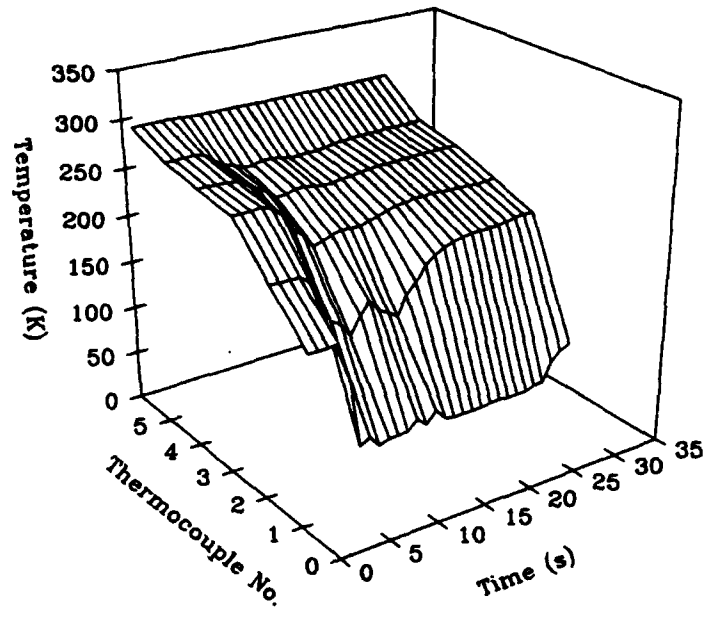

Nozzle: d=0.007"
Pressure in injector: 200 psig

Figure A.3 Transient Temperature Field

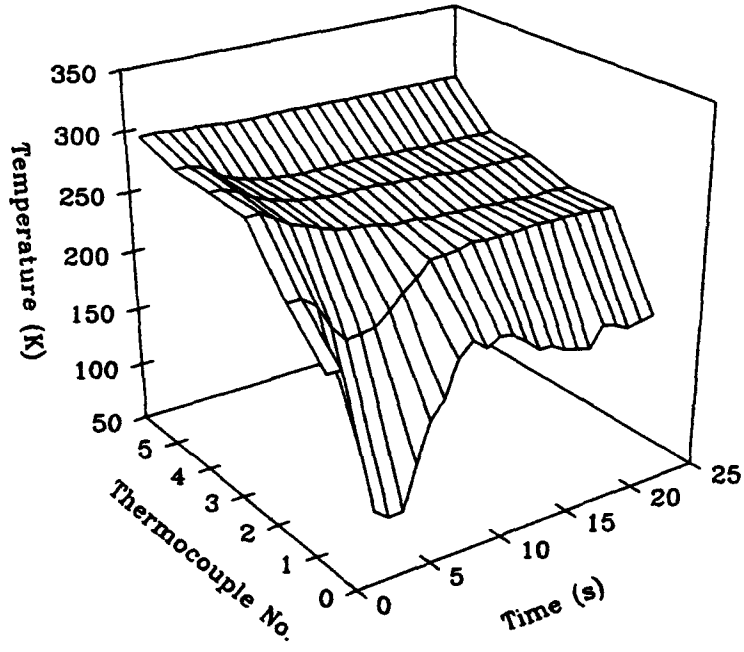

Nozzle: d=0.007"
Pressure in Injector: 400psig

Figure A.4 Transient Temperature Field

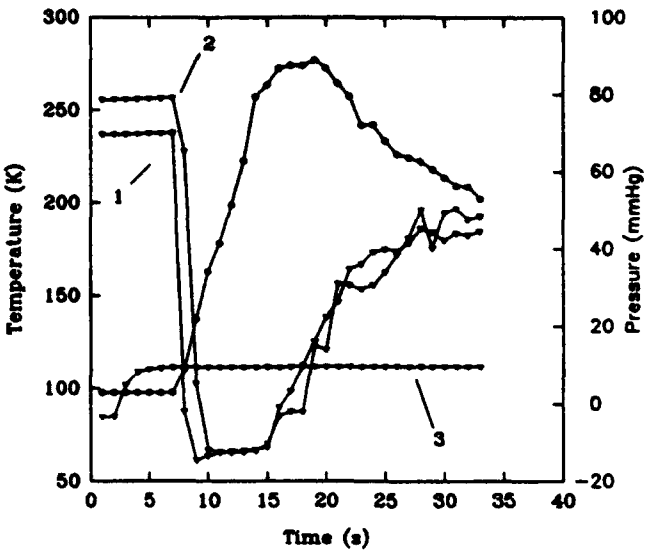

• –pressure
• –temperature
nozzle d= 0.010"
upstream pressure = 200psig
1–first thermocouple
2–second thermocouple
3–temperature in injector

Figure A.5 Temperature and Pressure in Blow-Down Tube

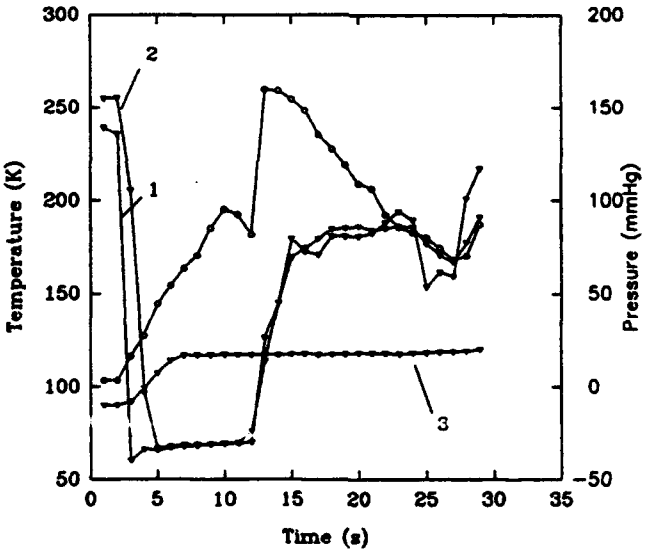

• –pressure
• –temperature
nozzle d= 0.010"
upstream pressure = 300psig
1–first thermocouple
2–second thermocouple
3–temperature in injector

Figure A.6 Temperature and Pressure in Blow-Down Tube

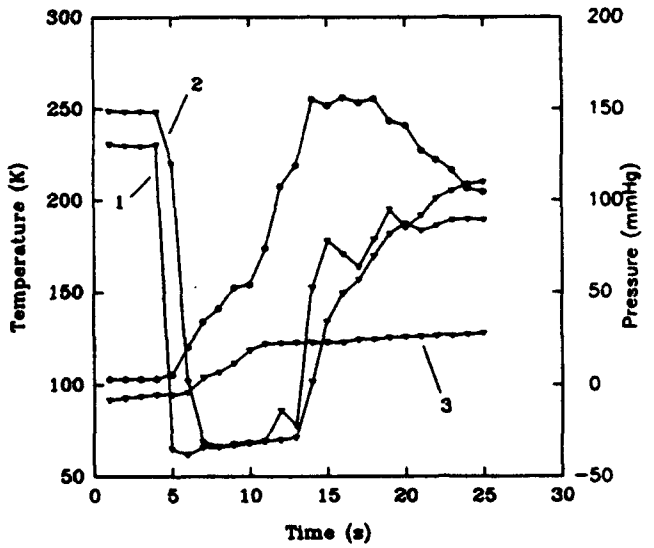

• -pressure
• -temperature
nozzle d= 0.010"
upstream pressure= 400psig
1-first thermocouple
2-second thermocouple
3-temperature in injector

Figure A.7 Temperature and Pressure in Blow-Down Tube

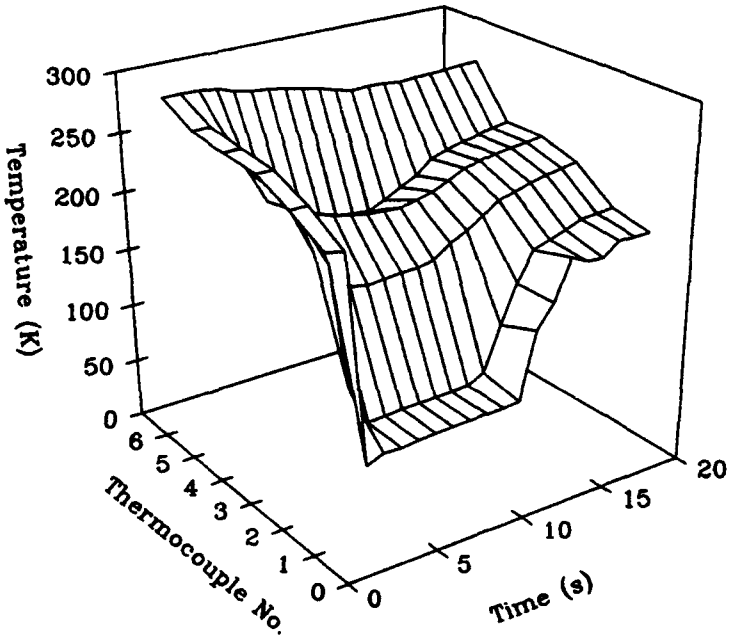

Nozzle: d=0.010"
Pressure in Injector: 300psig

Figure A.8 Transient Temperature Field

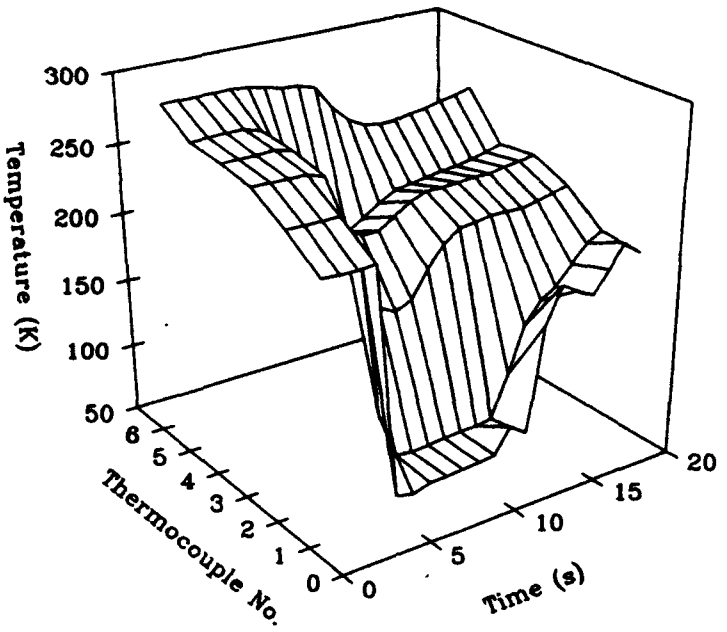

Nozzle: d=0.010"
Pressure in Injector: 400 psig

Figure A.9 Transient Temperature Field

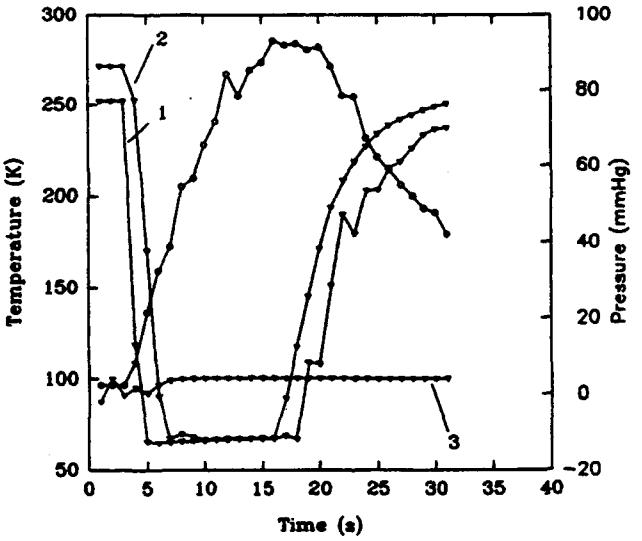

• –pressure
• –temperature
nozzle d= 0.014"
upstream pressure= 100psig
1–first thermocouple
2–second thermocouple
3–temperature in injector

Figure A.10 Temperature and Pressure in Blow-Down Tube

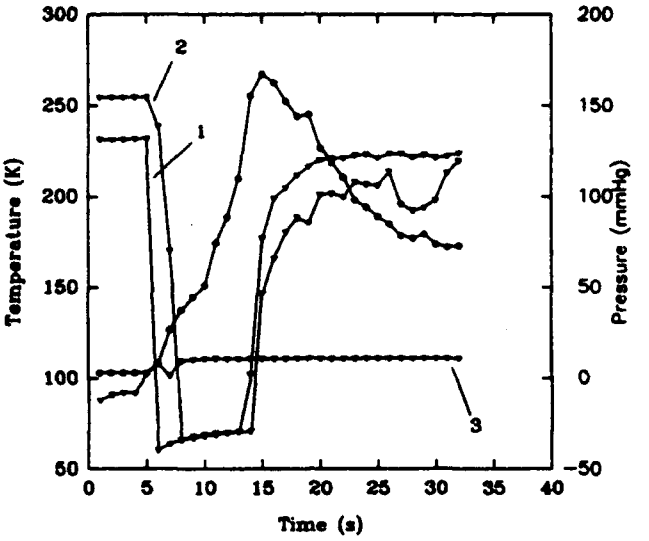

• -pressure
• -temperature
nozzle d= 0.014"
upstream pressure= 200psig
1-first thermocouple
2-second thermocouple
3-temperature in injector

Figure A.11 Temperature and Pressure in Blow-Down Tube

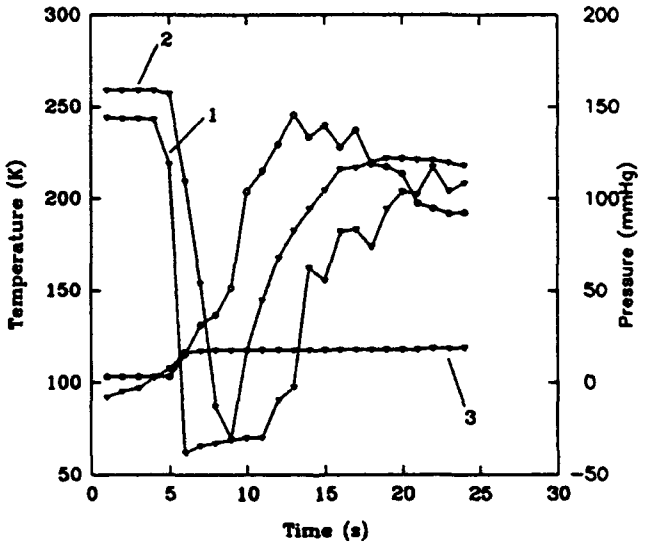

• -pressure
• -temperature
nozzle d= 0.014"
upstream pressure= 300psig
1-first thermocouple
2-second thermocouple
3-temperature in injector

Figure A.12 Temperature and Pressure in Blow-Down Tube

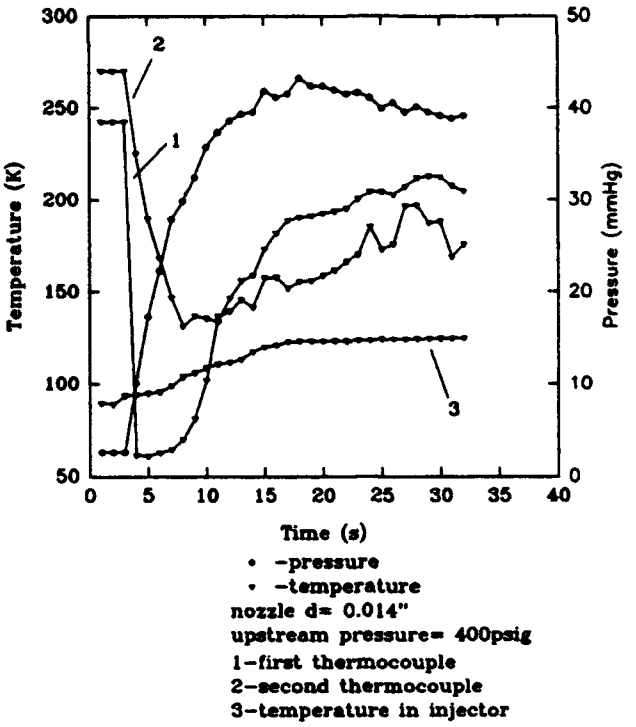

Figure A.13 Temperature and Pressure in Blow-Down Tube

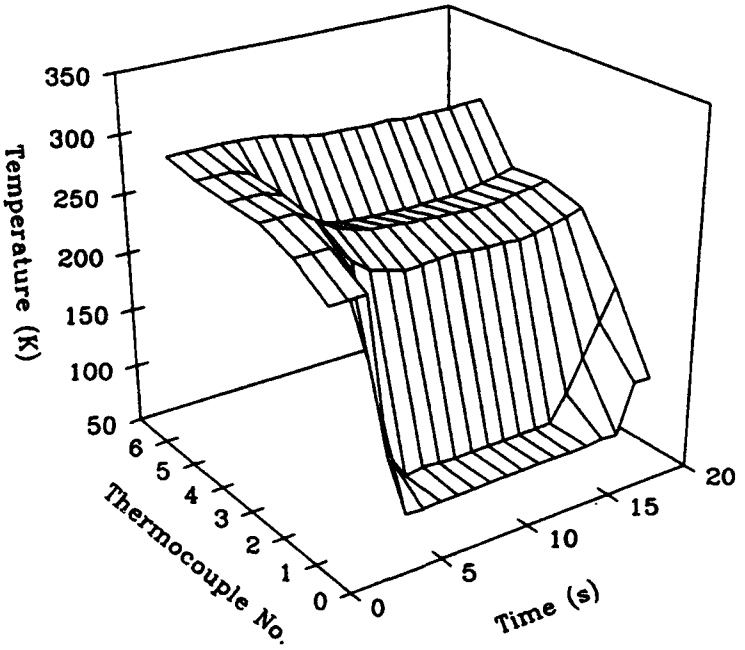

Nozzle: d=0.014"
Pressure in Injector: 100psig

Figure A.14 Transient Temperature Field

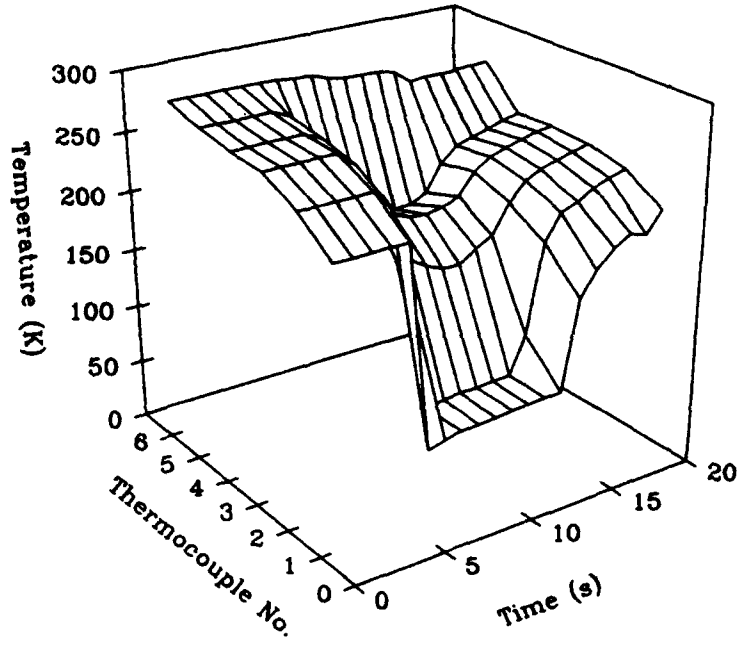

Nozzle: d=0.014"
Pressure in Injector: 200psig

Figure A.15 Transient Temperature Field

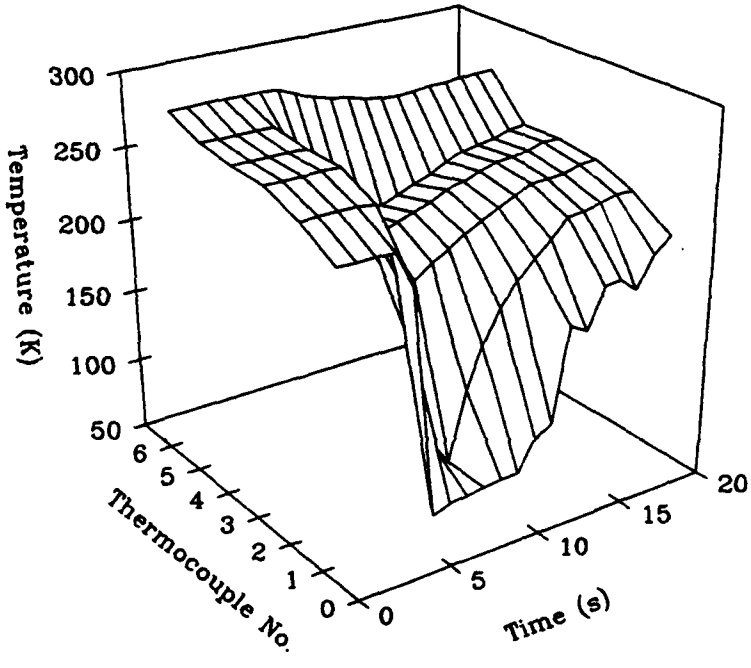

Nozzle: d=0.014"
Pressure in Injector: 300psig

Figure A.16 Transient Temperature Field

Figure A.17 Solid Nitrogen Being Pushed Out from Tube Nozzle

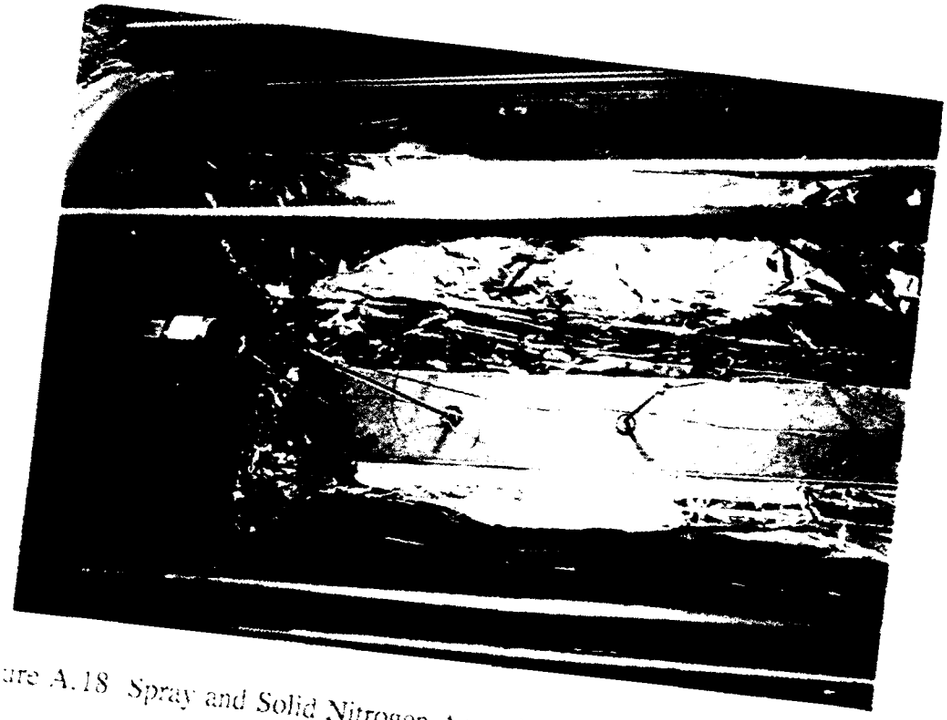

Figure A.18 Spray and Solid Nitrogen Accreting on Thermocouple (d=0.010")

Figure A.19 Large Nitrogen Block Accreted around Tube Nozzle

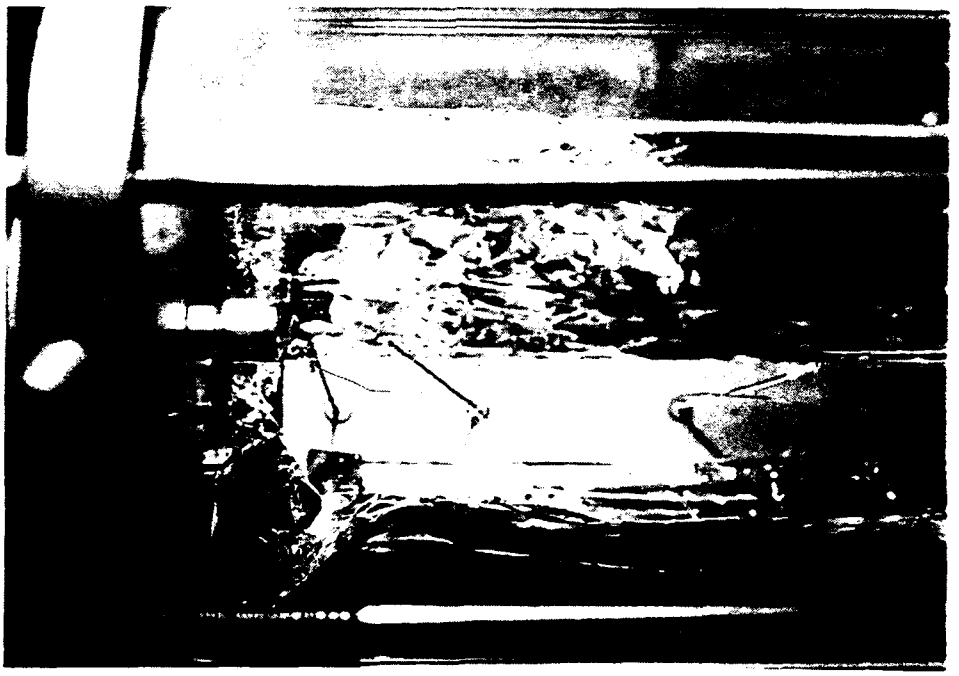

Figure A.20 Solid Nitrogen Being Blown Away from Thermocouple by Spray (d=0.020")